

# WFPC2 Imaging of Quasar Environments: A Comparison of LBQS and *HST* Archive Quasars<sup>1</sup>

Rose A. Finn, Chris D. Impey

*Steward Observatory*

*933 N. Cherry Ave., Tucson, AZ 85721*

`rfinn@as.arizona.edu, cimpey@as.arizona.edu`

and

Eric J. Hooper

*Harvard-Smithsonian Center for Astrophysics*

*60 Garden St., MS 83, Cambridge, MA 02138*

`ehooper@cfa.harvard.edu`

## ABSTRACT

We present *Hubble Space Telescope* (*HST*) Wide Field Planetary Camera 2 (WFPC2) data on the large-scale environments of 16  $0.39 < z < 0.51$  quasars from the Large Bright Quasar Survey (LBQS). The LBQS quasars are representative of the radio-quiet population, and this is the first look at their large-scale environments. We compare the LBQS environments with the environments of 27  $0.15 < z < 0.55$  quasars selected from the *HST* Archive. The majority of the Archive quasars are from the PG and PKS surveys, and these quasars are more luminous on average than the LBQS. By comparing the LBQS and Archive environments, we investigate whether previous quasar environment studies have been biased due to studying unusually radio or optically luminous quasars. We compare observed galaxy number counts with expected counts predicted from the CNOC2 field-galaxy luminosity function in order to look for statistical excesses of galaxies around the quasars. We detect a significant excess around the Archive quasars but find no such excess around the LBQS quasars. We calculate the amplitude of the spatial correlation function and find that the LBQS environments are consistent with that of the typical galaxy while the Archive environments are slightly

---

<sup>1</sup>Based on observations with the NASA/ESA *Hubble Space Telescope*, obtained at the Space Telescope Science Institute, which is operated by AURA, Inc.

less rich than Abell 0 clusters. We find no difference between the environments of radio-loud and radio-quiet quasars in either sample. However, comparison with previously published work shows that the LBQS radio-loud quasars are in sparse environments when compared with other radio-loud quasars, and the Archive radio-quiet quasars are in dense environments compared to other radio-quiet quasars. The richer environments of the Archive radio-quiet quasars can not be explained by their higher optical luminosities. We find a positive correlation (95%) between radio luminosity and environment for the radio-loud quasars. This may explain why the LBQS radio-loud quasars, which are less radio luminous, are in sparser environments.

*Subject headings:* quasars: general — galaxies: clustering: general — galaxies: interactions

## 1. INTRODUCTION

The conventional model explaining quasar activity consists of a supermassive black hole at the center of a galaxy. Accretion onto the black hole produces emission associated with the quasar, and interactions between the quasar host galaxy and its neighboring galaxies or intercluster gas help to keep the accretion disk and quasar fueled. The importance of interactions and mergers in triggering quasar activity is suggested by the high incidence of close companions (e.g. Weymann et al. 1978; Stockton 1982; French & Gunn 1983; Gehren et al. 1984; Malkan 1984; Yee & Green 1984; Yee 1987; Smith & Heckman 1990).

While the general quasar scenario is well-accepted, the origin of the radio power from quasars is still mysterious. Blandford (1990) suggests that the angular momentum of a spinning black hole, extracted by a magnetic field, can provide the energy necessary to fuel radio jets. This may imply that radio-loud quasars have black holes that spin more than radio-quiet quasars, and Wilson & Colbert (1995) show that a merger event between two black holes of relatively equal mass will result in a spinning black hole. Such a situation might arise if two spiral galaxies merge and subsequently form an elliptical galaxy. If the spiral galaxies harbor black holes of comparable mass, then the elliptical could possess a black hole with sufficient spin to power a radio-loud quasar.

Recent studies of the radio properties of quasars indicate that quasars do not exhibit a bimodal distribution of radio power, as originally thought (Brinkman et al. 2000). Radio-loudness is then more logically defined by radio luminosity, as opposed to the ratio of radio to optical luminosity. Various thresholds close to  $\log L = 24$  in units of  $\text{W Hz}^{-1} \text{sr}^{-1}$  (for  $H_0 = 50 \text{ km s}^{-1} \text{Mpc}^{-1}$ ) have been used to separate radio-loud and quiet quasars (e.g. Hooper et al. 1996; Bischof & Becker 1997; Goldschmidt et al. 1999), and we adopt this definition. According to this criteria, radio-loud quasars account for  $\approx 10\%$  of the entire quasar population.

Significant progress in understanding the mechanism responsible for radio emission will be

possible with X-ray satellites, such as XTXS. This telescope will be sensitive enough to detect signatures of the black hole rotation in iron K-line emission, so astronomers will be able to look for a correlation between black hole spin and radio power. Until then, a less direct but more tenable approach for understanding the radio properties of quasars focuses on quasar host galaxies and the large-scale environments of quasars. The first quasar host galaxy studies concluded that radio-loud quasars reside in elliptical hosts and radio-quiet quasars reside in spiral galaxies (Malkan 1984; Smith et al. 1986). More recent work shows that while radio-loud quasars are found mostly in elliptical hosts, radio-quiet quasars form in both elliptical and spiral galaxies (e.g. Bahcall et al. 1997; Boyce et al. 1998; McLure et al. 1999; Schade, Boyle, & Letawsky 2000). Quasar host studies require very precise observations and analysis, and larger samples are needed in order to learn what differentiates radio-loud and quiet quasars. The high contrast between nucleus and host and the small angular scale of the diffuse light make host studies very challenging.

Studies of the large-scale environments of quasars provide insight into the role of environment in triggering quasar activity and can be used to corroborate theories of radio power. The large-scale quasar environment can also be used as an indirect indicator of host morphology, according to the morphology-density relation that was first investigated by Dressler (1980). Dressler finds that local galaxy density is linked to galaxy type, namely, the fraction of elliptical and S0 galaxies increases with local galaxy density. From the beginning, quasar environment studies have searched for statistical excesses in galaxy counts around quasars, and we follow the same approach here. A more detailed understanding of the environments of individual quasars requires redshifts of faint galaxy companions.

This paper addresses two main questions. First, have previous quasar environment studies been biased by preferentially studying very strong radio sources or unusual optically selected quasars? Most studies from which the conventional picture of quasar environments was developed employ samples drawn mainly from the PG, PKS, 3C and 4C surveys (e.g. Yee & Green 1987; Ellingson et al. 1991). The radio surveys generally selected very luminous sources, which are quite rare in optical samples. Although the PG utilized selection techniques similar to other optically selected surveys, it is unusual in terms of its radio properties (e.g. La Franca et al. 1994; Hooper et al. 1996; Bischof & Becker 1997) and optical luminosity function (e.g. Wampler & Ponz 1985; Köhler et al. 1997; Goldschmidt & Miller 1998). Quasars from the Large Bright Quasar Survey (LBQS) are optically selected based on blue color, strong emission or absorption features, and a strong continuum break (Foltz et al. 1987). They are representative of the radio-quiet quasar population as a whole and are therefore more likely to reflect the incidence of clustering around quasars in general.

Second, are radio-loud quasars located in different environments than radio-quiet quasars? Yee and collaborators find that environment is linked to the radio properties of quasars. Radio-quiet quasars, while six times more likely to have a close companion than the average field galaxy (Yee 1987), are found in environments considerably less dense than those of radio-loud quasars (Yee & Green 1987; Ellingson, Yee, & Green 1991). Other studies with smaller samples show no evidence of

a correlation between radio properties and environment (e.g. Fisher et al. 1996; McLure & Dunlop 2000). In apparent contradiction, a recent study of  $0.5 \leq z \leq 0.8$  radio-loud quasars finds a slight but significant positive correlation between strength of environment and radio power (Wold et al. 2000). Clearly, the connection between environment and radio properties of quasars requires further investigation.

In this study, we present *HST* WFPC2 data on the environments of 43 quasars spanning the redshift range  $0.15 < z < 0.55$ , and we use this information to address the questions raised above. Although the field size of WFPC2 is relatively small, the superior resolution enables an accurate separation of stars from galaxies. This is a critical step in quantifying quasar environments. To investigate possible biases in quasar sample selection, we compare 16 LBQS quasars to a sample of quasars drawn from the Hubble Space Telescope (*HST*) Archive, consisting of mainly PG and PKS quasars. The LBQS and Archive samples contain 8 and 10 radio-loud quasars, respectively. We compare the environmental properties of the radio-loud and radio-quiet quasars within each sample and for the combined sample of LBQS and Archive quasars.

The layout of this paper is as follows. In Section 2, we discuss the details of the quasar samples and observations. In Section 3, we outline the procedure for photometry and source classification and compare the observed galaxy counts with expected counts derived from the CNOC2 luminosity function (Lin et al. 1999). We investigate the angular distribution of any observed excess counts (Section 3.3) and estimate the amplitude of the spatial correlation function for each quasar (Section 3.4). In Section 4, we discuss the significance of our results in the context of previous work, and Section 5 contains a summary. Cosmological parameters of  $H_0 = 100 \text{ km s}^{-1} \text{ Mpc}^{-1}$ ,  $q_0 = 0.5$ , and  $\Lambda = 0$  are assumed unless otherwise noted.

## 2. OBSERVATIONS AND DATA REDUCTION

Figure 1 shows  $M_V$  versus  $z$  for the entire set of 43 quasars in this environment study. Radio-loud and radio-quiet quasars are depicted with filled and open symbols, respectively. The LBQS (Hewett, Foltz, & Chaffee 1995) sample, shown with triangles in Figure 1, contains 16 quasars in the redshift range  $0.39 < z < 0.504$ , of which six are radio-loud. The remaining 10 quasars have 8.4 GHz luminosities less than  $10^{24} \text{ W Hz}^{-1} \text{ sr}^{-1}$  (for  $H_0 = 50 \text{ km s}^{-1} \text{ Mpc}^{-1}$ ). The 16 LBQS quasar fields were observed with *HST* in the *F675W* filter with WFPC2 during Cycle 4 with the quasar positioned on the PC, and an analysis of the quasar host properties is presented by Hooper, Impey, & Foltz (1997). For details on the observations, see Table 1 and Hooper et al. (1997).

Details of the observations for a comparison sample of 27 quasars drawn from the *HST* Archive can be found in Table 2. The 19 quasars observed in *F606W* are shown with squares in Figure 1. These quasars have lower redshifts, with  $0.15 < z < 0.29$ , and six of the 19 are radio-loud. All 19 *F606W* quasars were imaged on WF3. Studies of the host galaxies and large-scale environments of these quasars are presented by Bahcall et al. (1997) and Fisher et al. (1996), respectively. The

remaining 8 quasars of the Archive sample were observed in  $F702W$ ; 6 of the quasars were positioned on the PC and the other 2 on WF3. The redshifts range from  $0.223 \leq z \leq 0.514$ , and 4 out of 8 are radio-loud. References for the  $F702W$  data are listed in Table 2.

Figure 1 demonstrates that the combined quasar environment sample is free of the common correlation between absolute magnitude and  $z$ . A Spearman rank-correlation test confirms this, yielding a rank-correlation coefficient of 0.04, with an 80% probability of getting the same correlation from a random sample. Furthermore, a K-S test indicates with 84% significance that the absolute magnitudes for the radio-loud and radio-quiet quasars are drawn from the same parent population. However, a K-S test indicates only a 6% probability that the absolute magnitudes of the Archive and LBQS quasars are drawn from the same parent population, meaning that on average the Archive quasars are more luminous than the LBQS quasars.

For all quasar data, calibrated images are retrieved from the *HST* Archive, and cosmic ray rejection is achieved with the STSDAS combine routine with the “crreject” option set. Magnitude zeropoints for the three *HST* filters are from Table 9 in Holtzman et al. (1995). The zero points are adjusted for differences in gain and are increased by 0.1 to convert to infinite aperture magnitudes.

### 3. ANALYSIS

#### 3.1. Photometry and Geometry

SExtractor is used for photometry and source classification (Bertin & Arnouts 1996). For the wide-field cameras, a detection threshold of  $1.5\sigma$  per pixel is used with a minimum object size of 32 pixels. The PC images are binned by  $2 \times 2$  to improve signal-to-noise, and a detection threshold of  $1\sigma$  per pixel with a minimum object size of 32 pixels is used. Total magnitudes are determined using the “mag-auto” algorithm. A tophat  $5 \times 5$  convolution kernel is used for both the PC and WF data.

SExtractor does a remarkably good job at classifying objects in *HST* data. Figure 2 shows the SExtractor classification index versus magnitude for all of the  $F675W$  LBQS fields, where a classification index of 1 indicates a star or unresolved source and 0 a galaxy. We achieve a clean star/galaxy separation down to  $m_{F675W} = 22$  for the LBQS data. In Figure 2, the bright ( $m < 20$ ) objects in the LBQS PC fields with classifier indices between 0.5 and 0.95 correspond to the quasars, showing that a number of them are marginally resolved. The results of the star/galaxy separation are comparable for the Archive fields. We use a SExtractor classification index of 0.4 as our cut-off for galaxies. Note that the analysis is not sensitive to this value, since for  $m_{F675W} < 22$ , the distribution of classification indices is bimodal, with very few objects having indices greater than 0.1 and less than 0.9.

We determine the completeness of the data by adding artificial galaxies to the final images using the IRAF “artdata” package. Parameters for the artificial galaxies are based on data from Griffiths

et al. (1994a, 1994b) and include:  $1''$  for the maximum half-light radius of a  $m_{F675W} = 21$  elliptical galaxy, a value of one for the ratio of elliptical to spiral half-light radii, and 0.3 for the fraction of ellipticals. For the  $F675W$  data, we place artificial galaxies with  $20 \leq m_{F675W} \leq 23$  on the PC and WF images. We then estimate completeness based on how many of the artificial galaxies were recovered by SExtractor. In the 1200 second  $F675W$  data, 100% of  $21.5 \leq m_{F675W} < 22$  galaxies are recovered on the wide-field images. The results for the PC images are shown in Figure 3. The completeness drops to  $\sim 95\%$  for  $20.5 < m < 21.5$  galaxies and falls below 80% for  $21.5 < m < 22$  galaxies. To assess the significance of this incompleteness, we compute the expected galaxy counts per field (as discussed in Section 3.2). We find that the completeness-corrected counts do not differ significantly from the uncorrected counts down to  $m_{F675W} = 22$ . We therefore use  $m_{F675W} = 22$  as the faint magnitude cut for the  $F675W$  data and do not apply a completeness correction. The Archive data suffer from a similar level of incompleteness, so again we limit our analysis to  $m_{F606W} \leq 22$  and  $m_{F702W} \leq 22$  galaxies for the Archive quasars and make no other adjustments for completeness.

Before proceeding, we need to comment on the geometry of the images. First, all the LBQS quasars are centrally positioned on the PC. Six of the Archive quasars are also positioned on the PC, but the remaining 21 are located on WF3. Our results could be affected by the asymmetric geometry of WFPC2. For example, if a quasar positioned on the PC is located at the edge of a cluster, as found in a recent study of  $1.0 < z < 1.6$  radio-loud quasars (Sanchez & Gonzalez-Serrano 1999), we might miss the cluster entirely. The inferred environmental density will then be underestimated. We will be better able to comment on the effect of WFPC2 geometry when we analyze our wider-field, ground-based images of the LBQS quasars (see Section 5). Another issue that complicates any measure of local density around the quasars is the relatively small field size of WFPC2. At a redshift of 0.3, the  $2.5'$  field of WFPC2 corresponds to a projected size of  $0.58 h_{100}^{-1}$  Mpc, whereas the expected diameter of a group is  $\sim 1$  Mpc (e.g. Zabludoff & Mulchaey 1998). Therefore, for the lower-redshift quasars especially, we are sampling a limited volume around the quasar. Furthermore, since a group or cluster in which the quasar is located could fill the entire WFPC2 field, we cannot use the periphery of the images to estimate expected field-galaxy counts. These issues are addressed in the next section, with a direct comparison with wide-field galaxy counts.

### 3.2. Comparison of Galaxy Number Counts with Surveys

Our first step in looking for excess galaxies around the quasars is to compare the observed galaxy number counts with published surveys. This allows us to make a reliable estimate of expected galaxy counts even though a group or cluster in which a quasar is located may fill the entire WFPC2 field. Unfortunately, we find no deep galaxy surveys conducted in the three *HST* filters of interest. (The Medium Deep Survey includes  $F606W$  data, but number counts have not been published yet.) Converting number counts from other filters requires detailed knowledge of the galaxy populations

involved, which leads us to the CNOC2 dataset. Lin et al. (1999) have calculated the galaxy luminosity function based on CNOC2 data, and they parameterize the evolution of the luminosity function with redshift for both the  $B$  and  $R_C$  filters. Lin et al. (1999) classify galaxy SEDs using the Coleman, Wu, & Weedman (1980) templates, and knowing the percentage of different galaxy types allows one to transform the luminosity function parameters from  $R_C$  to any band, in our case the *HST*  $F606W$ ,  $F675W$  and  $F702W$  filters. To recover the integrated luminosity function for the *HST* filters, we use eq. (23) from Lin et al. (1999) and the  $R_C$  luminosity function parameters. We obtain the absolute  $R_C$  magnitudes from observed *HST* magnitudes by calculating the  $k$ - and color-corrections from the Coleman, Wu & Weedman SEDs. The zero point of each filter is determined from the spectrum of Vega. We integrate the luminosity function between  $0 < z < 1$ ; integrating beyond  $z = 1$  does not affect the counts below  $m = 22$ , but predicted counts at fainter magnitudes are affected.

As a test of the method, we calculate the integrated luminosity function for  $V$ ,  $R_C$  and  $F555W$  filters. Panels (a) through (c) of Figure 4 show that the integrated luminosity function reproduces the CNOC2  $V$  and  $R_C$  counts (H. Lin, private communication) as well as the Medium Deep Survey  $F555W$  counts (Casertano et al. 1995). The CNOC2 integrated luminosity function overpredicts the number of galaxies brighter than 19th magnitude. In terms of galaxies expected in a WFPC2 field with  $m_{R_C} < 22$ , the integrated luminosity function predicts 32.6 galaxies per field while the CNOC2 counts give 31.5 galaxies per field. In the  $V$  band, an average of 16.2 galaxies are expected and 16.0 are observed. This means that in our  $F675W$  and  $F702W$  quasar fields, the expected field galaxy counts will be systematically high by  $\approx 1$  galaxy per field. For the  $F606W$  data, which are closer to  $V$ , the expected field galaxy counts will be systematically high by  $< 0.5$  galaxy per field.

Our next step in looking for excess galaxies is to use the CNOC2 integrated luminosity function to estimate the expected galaxy counts in the quasar fields. Implicit in this comparison is the assumption that the magnitudes derived from SExtractor are equivalent to the CNOC2 galaxy magnitudes. The CNOC2 galaxy magnitudes are determined using the PPP software (Yee 1991). To check the validity of this assumption, H. Lin ran SExtractor and PPP on the same data. A comparison of the SExtractor and PPP total magnitudes shows  $\sim 0.2$  magnitudes of scatter but no systematic offset (H. Lin, private communication). We therefore proceed in using the CNOC2 integrated luminosity function to predict the expected galaxy counts in the quasar fields.

The CNOC2 luminosity function is integrated for the *HST*  $F675W$ ,  $F606W$  and  $F702W$  filters, and the results are plotted with the galaxy counts from the quasar fields in panels (d) through (f) of Figure 4. The integrated  $F675W$  luminosity function reproduces the observed galaxy counts from the LBQS fields within the errors down to  $m \approx 23$ . The  $F606W$  Archive galaxy counts show a clear excess at magnitudes brighter than 21, but the integrated luminosity function matches the faint galaxy counts well. The  $F702W$  Archive galaxy counts show a slight excess above the predicted counts at almost all magnitudes.

To assess the significance of these findings, we translate from galaxies per square degree per magnitude into the average expected and observed counts per field. To determine the expected galaxy counts per field, we sum the integrated luminosity function between  $14 < m < 22$  and multiply by the area of WFPC2 in square degrees. This pushes slightly beyond the spectroscopic completeness level of  $R_C = 21.5$  for the CNOC2 survey. The observed, expected, and excess counts for the individual LBQS fields are listed in columns 5, 6 and 7 of Table 3. The same quantities are listed for the *F606W* and *F702W* Archive fields in Tables 4 and 5. We find that the LBQS quasars have an average of 16.1 galaxies per field,  $1.8 \pm 1.4$  galaxies less than expected. The Archive *F606W* and *F702W* quasars have an average of 16.4 and 26.5 galaxies per field,  $5.4 \pm 1.0$  and  $7.0 \pm 2.0$  galaxies more than expected, respectively. The error in the excess counts is determined by propagating the error in expected counts. The error in expected counts is taken to be 1.3 times the Poisson error, where the extra factor of 1.3 accounts for variations associated with large-scale structure, as observed by Yee, Green, & Stockman (1986). We see no significant excess associated with the LBQS quasars. The Archive quasars, in comparison, have very significant excesses. The average excess of 5.4 galaxies per field associated with the *F606W* Archive quasars is a total that is slightly more than  $5\sigma$  above the noise associated with the expected galaxy counts. The average excess of 7.0 galaxies per field detected in the *F702W* Archive images is a  $3\sigma$  result overall.

Previous quasar environment studies have limited the analysis to galaxies with  $m < m_* + 2.5$  (Yee & Green 1987) or  $m_* - 1 < m < m_* + 2$  (Fisher et al. 1996; McLure & Dunlop 2000), where  $m_*$  is the apparent magnitude of the knee of the luminosity function at the redshift of each quasar. This acts to reduce the contamination from field galaxies. Since all of the *F606W* Archive fields are common to the Fisher et al. dataset, we apply a magnitude slice of  $m_* - 1 < m < m_* + 2$  to facilitate comparison. For consistency with the estimation of expected counts, we use the value of  $m_*$  derived from CNOC2. Values of  $m_*$  are listed in column 10 of Tables 3, 4, and 5 for the LBQS, *F606W*, and *F702W* Archive quasars, respectively. In addition, the observed, expected, and excess number of galaxies are listed in columns 11, 12, and 13. Applying this limited magnitude slice leaves the average observed excess for the LBQS fields unchanged:  $-1.8 \pm 1.4$  becomes  $-1.7 \pm 1.4$  galaxies. The negative sense of the average for the LBQS sample is not significant. The excess for the *F606W* Archive fields drops from  $5.4 \pm 1.0$  to  $3.7 \pm 0.7$  galaxies per field. The excess for the *F702W* Archive fields drops from  $7.0 \pm 2.0$  to  $5.8 \pm 1.8$  galaxies per field. This restricted magnitude slice does not change the significance of the observed excesses.

### 3.3. Radial Distribution of Galaxies

We detect an excess of galaxies above the CNOC2-derived field estimate in the Archive data. We observe no significant excess in counts in the LBQS fields. If we assume that the excess galaxies observed in the Archive fields are associated with the quasar and are located at the quasar redshift, then we might expect the excess counts to originate from regions close to the quasar, as seen in other studies (e.g. Yee & Green 1987; Ellingson et al. 1991; Smith, Boyle, & Maddox 1995; Fisher et



al. 1996; Hall & Green 1998). Figure 5 shows the average excess number of galaxies per field versus angular distance from the quasar for the Archive and LBQS samples. The Archive fields show an excess with no obvious radial dependence, and the LBQS show no excess. Since the Archive quasars span a large range in redshift, a given angular distance corresponds to a very different projected distance for the lowest and highest redshift Archive quasars. This could dilute an observed radial gradient of galaxies. Therefore, in Figure 6 we plot the spatial distribution of excess galaxies. Here we assume that all the galaxies in the field are at the quasar redshift and convert angular distance to projected physical distance. Counts are binned in equal-width annuli of  $100 h_{100}^{-1}$  kpc. This comparison shows a highly significant excess of galaxies out to  $400 h_{100}^{-1}$  kpc for the Archive quasars and no excess for the LBQS quasars. The difference between Figures 5 and 6 for the Archive data supports the assumption that the excess galaxies are associated with the quasar. The significance of the drop-off in excess counts at radii larger than  $300 h_{100}^{-1}$  kpc is difficult to assess due to the limited field size of WFPC2.

In looking for a radial gradient in galaxy counts around a given quasar, we are assuming that the quasar is at the center of the local mass concentration. A recent study of higher-redshift quasars shows that this is not necessarily the case (Sanchez & Gonzalez-Serrano 1999). Unfortunately, the WFPC2 field is not big enough to explore this scenario. The possibility that quasars are not centered in their groups or clusters will be addressed with existing ground-based data for the LBQS sample, and these results will be presented in a future paper.

### 3.4. Amplitude of the Spatial Correlation Function

One common way to quantify the strength of clustering around quasars is to calculate the amplitudes of the angular and spatial correlation functions. For a given cluster around a quasar, the amplitude of the angular correlation function,  $A_{gq}$ , will decrease with increasing quasar redshift. The amplitude of the spatial correlation function,  $B_{gq}$ , takes redshift into account by projecting angular distances into physical distances. Therefore,  $B_{gq}$  is a better way to compare our samples. However,  $A_{gq}$  is the parameter that is measured observationally. Longair & Seldner (1979) derived the relation between  $A_{gq}$  and  $B_{gq}$ , and a brief summary of their work is given below.

The angular correlation function,  $\omega(\theta)$ , is defined by

$$n(\theta) d\Omega = n_{exp} (1 + \omega(\theta)) d\Omega, \quad (1)$$

where  $n(\theta)$  and  $n_{exp}$  are the surface densities of observed and expected galaxies, respectively, and  $d\Omega$  is surface area. The spatial correlation function,  $\xi(r)$ , is defined as the excess number of galaxies at a distance  $r$  from an object in a volume element  $dV$ ,

$$\rho(r) dV = \rho_{exp} (1 + \xi(r)) dV. \quad (2)$$

The quantities  $\rho(r)dV$  and  $\rho_{exp}dV$  are the number of galaxies observed and expected in volume element  $dV$ , respectively. Longair & Seldner (1979) show that  $\xi(r) = B_{gq} r^{-\gamma}$  implies  $\omega(\theta) =$

$A_{gq} \theta^{-(\gamma-1)}$ . In deriving the relationship between  $A_{gq}$  and  $B_{gq}$ , Longair & Seldner (1979) find

$$B_{gq} = \frac{A_{gq} n_{exp}}{\phi(m_o, z) \left(\frac{D}{1+z}\right)^{3-\gamma} I_\gamma}, \quad (3)$$

where  $\phi(m_o, z)$  is the luminosity function integrated at the quasar redshift down to limiting magnitude  $m_o$ ,  $D$  is the effective distance (making  $D/(1+z)$  the angular diameter distance,  $D_A$ ), and  $I_\gamma$  is the integration constant that arises from integrating the volume in a cone corresponding to surface area  $d\Omega$ .

In practice, in order to calculate  $B_{gq}$ , we must first calculate  $A_{gq}$ . Substituting the functional form of  $\omega(\theta)$  from Longair & Seldner (1979) into equation 1, integrating  $d\Omega$  over the image area and solving for  $A_{gq}$ , we find

$$A_{gq} = \frac{N_{obs} - N_{exp}}{n_{exp} \sum \theta^{-(\gamma-1)} \Delta\Omega}. \quad (4)$$

The final expression for  $B_{gq}$ , obtained by substituting equation 4 into equation 3, is

$$B_{gq} = \frac{N_{obs} - N_{exp}}{\phi(m_o, z) D_A^{(3-\gamma)} I_\gamma \sum \theta^{-(1-\gamma)} \Delta\Omega}. \quad (5)$$

If we consider only the Poisson error associated with  $N_{exp}$  and  $\phi(m_o, z) D_A^3$ , the uncertainty in  $B_{gq}$  is

$$\frac{\Delta B_{gq}}{B_{gq}} = \frac{1}{N_{obs} - N_{exp}} \sqrt{1.32 N_{exp} + \frac{(N_{obs} - N_{exp})^2}{\phi(m_o, z) D_A^3}}. \quad (6)$$

In calculating  $B_{gq}$ , we use  $\gamma = 1.77$ , the power law index derived from local studies of the galaxy-galaxy covariance function (Seldner & Peebles 1978). Yee & Green (1987) demonstrate that  $\gamma = 1.77$  is appropriate to use for  $z < 0.6$  quasars. This makes the units of  $B_{gq}$   $\text{Mpc}^{1.77}$ . We evaluate  $\sum \theta^{-\gamma} \Delta\Omega$  by summing  $\Delta\Omega$  in concentric, quasar-centered annuli from zero radius to the most distant point in the field. The field counts,  $N_{exp}$ , are derived from the CNOC2 luminosity function (Lin et al. 1999) as described in Section 3.2. We also use the CNOC2 luminosity function for calculating  $\phi(m_o, z)$ .

The results of the  $B_{gq}$  calculations are listed in Tables 3, 4, and 5 for the LBQS, *F606W*, and *F702W* Archive samples. The layouts of Tables 3, 4, and 5 are identical. Columns 1 and 2 give the quasar name and redshift. The angular distance from the quasar to the furthest corner of the WFPC2 field is listed in column 3, and the physical distance that this angle corresponds to at the quasar redshift,  $r_{max}$ , is listed in column 4. Columns 5 through 9 correspond to all galaxies within the magnitude range  $14 < m < 22$ . Columns 5 and 6 give the total number of observed and expected galaxies per WFPC2 field. The error in the expected counts are 1.3 times the Poisson error, as described in Section 3.2. Column 7 gives the excess number of galaxies per field, and column 8 expresses this excess in terms of  $\delta$ , the ratio of the excess counts to the expected counts. Column 9 lists the calculated values of  $B_{gq}$ , with the errors derived according to equation

6. Columns 10 through 15 refer to only those galaxies with  $m_* - 1 < m < m_* + 2$ . Column 10 gives the value of  $m_*$  for each quasar, and columns 11 through 15 are analogous to columns 5 through 9, but for the narrower magnitude range.

The average  $B_{gq}$  for the LBQS sample is  $-16 \pm 13 (h_{100}^{-1} \text{ Mpc})^{1.77}$ . As with the average number counts for the LBQS sample, the negative sense of the average  $B_{gq}$  value is not significant. The average values of  $B_{gq}$  for the *F606W* and *F702W* Archive samples are  $59 \pm 11$  and  $58 \pm 18 (h_{100}^{-1} \text{ Mpc})^{1.77}$ . Considering  $m_* - 1 < m < m_* + 2$  galaxies only leaves the average value of  $B_{gq}$  unchanged for the LBQS sample. The averages for the *F675W* and *F702W* Archive samples are  $60 \pm 10$  and  $49 \pm 18 (h_{100}^{-1} \text{ Mpc})^{1.77}$ . For comparison, Davis & Peebles (1983) find that the average value for the amplitude of the galaxy-galaxy spatial correlation function,  $B_{gg}$ , is  $20 (h_{100}^{-1} \text{ Mpc})^{1.77}$ , and Longair & Seldner (1979) find that clusters with Abell richness classes 0 and 1 have  $B_{gg}$  values of 90 and 250  $(h_{100}^{-1} \text{ Mpc})^{1.77}$ , respectively. The LBQS quasar environments are consistent with that of a typical galaxy, while the average Archive quasar environment is slightly less rich than an Abell 0 cluster. We note that the relative values and significance levels of  $B_{gq}$  for the various samples match the simple estimates of galaxy excess with respect to published surveys, as expected.

Since our quasar sample spans a wide range of redshifts, measuring  $B_{gq}$  out to the edge of the field could introduce systematic differences in the results calculated for low and high-redshift quasars. To make the measurements more uniform, we recalculate  $B_{gq}$  for galaxies within a projected distance of  $200 h_{100}^{-1} \text{ kpc}$  from the quasar. This corresponds to the largest physical size imaged by WFPC2 for the lowest redshift quasar in the Archive sample. For  $14 < m < 22$  galaxies only, the average value of  $B_{gq}$  for the LBQS sample is  $0 \pm 11 (h_{100}^{-1} \text{ Mpc})^{1.77}$ . The average values for the *F675W* and *F702W* Archive samples are  $53 \pm 10$  and  $65 \pm 16 (h_{100}^{-1} \text{ Mpc})^{1.77}$ . These values do not change significantly when considering only galaxies with  $m_* - 1 < m < m_* + 2$ . Thus, the distance at which  $B_{gq}$  is measured does not affect the average  $B_{gq}$  values significantly. Unless otherwise stated, we will refer to the  $B_{gq}$  values calculated for  $m_* - 1 < m < m_* + 2$  galaxies using the entire WFPC2 field for the remainder of the paper.

Figure 7 shows a plot of  $B_{gq}$  versus redshift, and three interesting points emerge from this figure. First, we find no apparent radio dichotomy. A K-S test indicates that the radio-loud and radio-quiet samples are drawn from the same population with 58% confidence. Similar results are obtained for the three subsamples individually; for the LBQS, *F606W*, and *F702W* Archive fields, a K-S test indicates a 70%, 56% and 53% probability that the radio-loud and radio-quiet subsamples are drawn from the same distribution of  $B_{gq}$  values. The similarity of radio-loud and radio-quiet environments is consistent with results of Fisher et al. (1996) and McLure & Dunlop (2000) but is not consistent with the findings of Ellingson et al. (1991). We will discuss this point in more detail in Section 4.

The second point to draw from Figure 7 is that the values of  $B_{gq}$  for the LBQS sample lie systematically below those of the Archive quasars. The significance of this difference is 99%, as determined by the K-S test. This is consistent with the differences found between the LBQS and

Archive samples based on number counts, described in Section 3.2. Is something different about the LBQS environments, or is there some systematic error associated with the LBQS data or analysis? One possible systematic is the shorter exposure times of the LBQS data. Therefore, we might not be sampling far enough down the luminosity function to pick up companions. By applying a limiting magnitude cut of  $m_{F675W} = 22$ , we sample to an average depth of  $m_* + 1.4$  in the LBQS data. To see how this shallower depth affects the inferred environmental density, we recalculate  $B_{gq}$  for the Archive fields using only  $m_* - 1 < m < m_* + 1.4$  galaxies. The resulting  $B_{gq}$  values are plotted versus quasar redshift in Figure 8. A K-S test again indicates only a 0.6% probability that the  $B_{gq}$  values for LBQS and Archive quasars are drawn from the same parent distribution. We must then conclude that the LBQS quasars are located in environments less dense than the Archive quasars.

The final conclusion drawn from Figures 7 and 8 is that we do not see an increase in  $B_{gq}$  with increasing redshift out to  $z = 0.5$ . Hill & Lilly (1991) see a significant enhancement in the environments of radio galaxies with moderate to high radio power by  $z \sim 0.5$ , and Yee & Green (1987) find evidence for a strong increase in the density of environments of radio-loud quasar at  $z > 0.6$ . A Spearman rank test performed on the data in Figure 8 indicates a negative correlation between  $B_{gq}$  and  $z$  at the 99% confidence level. However, this correlation disappears when considering the Archive data only, with a Spearman rank test indicating an 86% probability that no correlation exists. Therefore, the correlation of  $B_{gq}$  with  $z$  is due to the systematically lower  $B_{gq}$  values of the higher-redshift LBQS quasars.

#### 4. DISCUSSION

In this section, we discuss our analysis and results in the context of previous work. We can compare our analysis of the *F606W* Archive data with that of Fisher et al. (1996) because we utilize the exact same data for 19 of the 20 quasars they imaged. Our radio-loud subsamples are identical, while Fisher et al. include one more quasar (HE 1029–1401 at  $z = 0.086$ ) in their radio-quiet subsample. Fisher et al. do not list any individual statistics; we know only that the average value of  $B_{gq}$  for their entire sample, considering only  $m_* - 1 < m < m_* + 2$  galaxies, is  $75_{-15}^{+18} (h_{100}^{-1} \text{ Mpc})^{1.77}$ . For the same magnitude slice, our value is  $60 \pm 10 (h_{100}^{-1} \text{ Mpc})^{1.77}$ . For the radio-loud and radio-quiet subsamples, their average values of  $B_{gq}$  are  $84_{-27}^{+33}$  and  $72_{-19}^{+20} (h_{100}^{-1} \text{ Mpc})^{1.77}$ , respectively. In comparison, our values are  $66 \pm 18$  and  $57 \pm 12 (h_{100}^{-1} \text{ Mpc})^{1.77}$ . Although our results agree within the errors, our  $B_{gq}$  values are systematically lower than the Fisher et al. values. The discrepancies translate into a difference of  $\sim 1$  galaxy in the calculated average excess. Differences in how the expected counts are estimated can probably account for the differences in  $B_{gq}$  values. For example, as mentioned in Section 3.2, the background counts estimated from the CNOC2 luminosity function may be systematically high by  $< 0.5$  galaxy per field for the *F606W* filter. In addition, Fisher et al. do not use the PC data in their analysis, and they estimate the expected counts in WF3 using the observed counts in WF2 and WF4.

Another useful check of our analysis is to compare individual  $B_{gq}$  values with those published by other authors. McLure & Dunlop (2000) also analyze the  $F606W$  sample, and four of those quasars are common to Yee & Ellingson (1993). Table 6 compares  $B_{gq}$  for these four quasars plus one additional  $F702W$  quasar that is not in the McLure & Dunlop sample but is in the Yee & Ellingson sample. The agreement between our values and those of Yee & Ellingson (1993) is surprisingly good, considering the following differences: they use ground-based data covering a much wider field than WFPC2; they estimate field galaxy counts from control fields; and they use different parameters for calculating the luminosity function at the quasar redshift. McLure & Dunlop (2000) have analyzed the same  $HST$  data as we, so one might expect better agreement between our  $B_{gq}$  values. However, McLure & Dunlop (2000) consider only galaxies located on the same chip as the quasar (WF3) and estimate expected counts based on the number of galaxies on WF2 and WF4. Furthermore, they use different parameters when calculating the luminosity function at the quasar redshift. This comparison underscores how sensitive individual  $B_{gq}$  values are to the methodology and indicates that results should only be interpreted in a statistical sense.

Finding reasonable agreement among our analysis and those of Fisher et al. (1996), McLure & Dunlop (2000), and Yee & Ellingson (1993), we now discuss the significance of our findings in the context of previous research. Our two main results are that 1) the LBQS quasars lie in less dense environments than the more luminous Archive quasars, and 2) radio-loud and radio-quiet quasars are found in similar environments. Table 7 compares our average values of  $B_{gq}$  to those of other studies. Note that the Archive  $F606W$  and Fisher et al. (1996) data and samples are identical except for one quasar, and McLure & Dunlop (2000) include all the  $F606W$  quasars in their sample. With this in mind, comparing  $B_{gq}$  values puts the findings of this study in a different light. First, the relatively sparse environments of the radio-quiet LBQS quasars are consistent with previous ground-based studies, but the radio-loud LBQS quasars are in unusually sparse environments when compared to other radio-loud quasars. Second, the richer environments of the Archive radio-loud quasars are consistent with previous ground-based studies, but the Archive radio-quiet quasars are in unusually dense environments compared with the radio-quiet quasars studied by Smith et al. (1995) and Ellingson et al. (1991). Furthermore, by comparing our values of  $B_{gq}$  to the Longair & Seldner (1979) value of  $90 (h_{100}^{-1} \text{ Mpc})^{1.77}$  for Abell 0 clusters, we find that the Archive quasars are located in galaxy environments slightly less rich than Abell 0 clusters. When compared with the galaxy-galaxy covariance amplitude of  $20 (h_{100}^{-1} \text{ Mpc})^{1.77}$  from Davis & Peebles (1983), the LBQS quasars are in environments comparable to the typical galaxy. This is not surprising for the radio-quiet LBQS subsample, but one might expect the radio-loud LBQS quasars to be in denser environments.

How do we make sense of these results? Fisher et al. (1996) note that the  $F606W$  quasars are among the most luminous, and this might explain why the  $F606W$  radio-quiet quasars have denser environments than average. Furthermore, the LBQS quasars are less luminous on average than the Archive quasars, so maybe this explains why the LBQS are in relatively sparse environments. Figure 9 compares  $B_{gq}$  with  $M_V$ , showing clearly that environment is not correlated with optical luminosity.

A Spearman rank test confirms this with a 60% probability that  $B_{gq}$  and  $M_V$  are uncorrelated. Ellingson et al. (1991) look for a correlation between optical luminosity and environment with a sample of 96 quasars, and they also find no correlation. Therefore, it appears that optical luminosity can not explain why the Archive radio-quiet are in dense environments nor why the LBQS radio-loud quasars are in sparse environments. Radio luminosity might help explain the sparse environments of the radio-loud LBQS quasars because the radio-loud LBQS quasars have lower radio luminosities than the Archive radio-loud quasars. To test this we compare radio power at 5 GHz with  $B_{gq}$ . Radio power is listed in Tables 1 and 2 for the LBQS and Archive quasars, respectively. The LBQS 8.4 GHz data from Hooper et al. (1997) are converted to 5 GHz using a spectral index of  $-0.32$ . Radio data for the *F606W* sample are from McLure & Dunlop (2000), and data for the *F702W* sample are from NASA/IPAC Extragalactic Database.

Figure 10 shows  $B_{gq}$  versus radio power, and we find no correlation between radio power and environment when considering both radio-loud and quiet quasars. We note that almost all the LBQS quasars are a factor of 10-100 less powerful than the radio-loud Archive quasars, and it is not clear that the same emission mechanism holds across this large range in radio power. However, when considering the radio-loud quasars only, a Spearman rank test indicates a modest correlation (95% probability) between radio power and environment, which is dependent on the one point at extreme values of radio luminosity and  $B_{gq}$  (85% probability of a correlation if this point is removed). Wold et al. (2000) find a slight but significant correlation between radio power and environment, although they consider steep spectrum sources only. Most of the radio-loud quasars in our samples are flat spectrum, yet the correlation remains. Interestingly, McLure & Dunlop (2000) note that a weak trend between radio power and environment is suggested by their data, but the correlation is not statistically significant. The richest environments in the Yee & Green (1987) and Ellingson et al. (1991) samples are around very radio luminous, steep-spectrum sources. The addition of their data to Figure 10 might strengthen the correlation between environment and radio power, but we resist adding their numbers due to possible systematic differences in analysis. Since most of the radio data for the radio-quiet quasars are upper limits, we cannot test for an independent correlation between radio power and environment for radio-quiet quasars. The fact that the correlation in the radio-loud data does not apply to both radio-loud and quiet quasars implies that two emission mechanisms may be at work (e.g. Stocke et al. 1992; Hooper et al. 1996), even though there appears to be a continuum of radio power among quasars.

Finally, what is the true incidence of clustering around quasars? As discussed in Section 1, the LBQS is among the most representative surveys of the currently known radio-quiet quasar population, and the radio-quiet quasars make up  $\approx 90\%$  of the whole. Therefore, most quasars, like the LBQS sample presented here, lie in environments comparable to the typical galaxy. The Archive radio-quiet quasars have unusually dense environments and are thus not a representative sample of radio-quiet quasars. The clustering associated with radio-loud quasars correlates with radio power, and the environments of the radio-loud quasars presented here range from that of a typical galaxy to Abell 0 clusters. We present data for only 16 LBQS quasars, and a larger sample is

needed to strengthen these results. In addition, spectroscopic studies provide more insight into the dynamics of quasar environments, enabling one to examine variations in environments as opposed to limiting analysis to the average properties of the sample. The fluctuations in field galaxy counts preclude the analysis of individual quasars using our current method.

The LBQS makes an excellent sample for extending quasar environment studies to higher redshift to look for evolution. This work has been started by Wold et al. (2001), who include 10 LBQS radio-quiet quasars in their study of  $0.5 \leq z \leq 0.8$  radio-quiet quasar environments. Wold et al. (2001) conclude that, on average,  $0.5 \leq z \leq 0.8$  radio-quiet are found in environments that are  $3\times$  more dense than the typical galaxy. However, the 10 LBQS quasars in their radio-quiet sample have environments comparable to the typical galaxy (for their star-subtraction Models 2 and 3). We have ground-based  $R$  and  $H$ -band data for a larger sample of LBQS quasars, which includes the sample presented here as well as higher redshift quasars. The ground-based data are much deeper than the *HST* data, and their analysis will help elucidate the true incidence of clustering around quasars as a function of redshift.

## 5. SUMMARY

We present *Hubble Space Telescope* (*HST*) Wide Field Planetary Camera 2 (WFPC2) data on the large-scale environments of 16  $0.39 < z < 0.51$  quasars from the Large Bright Quasar Survey (LBQS). This is the first look at the large-scale environments of LBQS quasars, and this is significant because the LBQS quasars are representative of the radio-quiet quasar population. We compare the LBQS environments with the environments of 27  $0.15 < z < 0.55$  quasars selected from the *HST* Archive. The analysis of the Archive sample is useful for two reasons. First, the Archive sample provides a check of our methodology because most of these data have been published in previous environment studies. Second, the majority of the Archive quasars are from the PG and PKS surveys, and these quasars are more luminous on average than the LBQS quasars; by comparing the LBQS and Archive studies we investigate whether previous quasar environment studies have been biased due to studying unusually radio or optically luminous quasars. To quantify the quasar environments, we compare observed galaxy number counts with expected counts predicted from the CNOC2 field-galaxy luminosity function in order to look for statistical excesses of galaxies around the quasars. We detect a significant excess of galaxies around the Archive quasars but find no such excess around the LBQS quasars. We calculate the amplitude of the spatial correlation function, and we find that the LBQS environments are consistent with that of the typical galaxy while the Archive environments are slightly less rich than Abell 0 clusters. Contrary to previous ground-based studies, we find no difference between the environments of radio-loud and radio-quiet quasars of either sample. However, comparison of  $B_{gq}$  values with previously published values shows the radio-loud LBQS quasars are in environments less dense than most other radio-loud quasars. In addition, the Archive radio-quiet quasars are in anomalously dense environments compared to other radio-quiet quasars. The richer environments of the Archive radio-quiet quasars can not

be explained by their higher optical luminosities because we find no correlation between optical luminosity and environment. We do find a positive correlation (95%) between radio luminosity and environment for the radio-loud quasars. The LBQS radio-loud quasars have lower radio powers than the radio-loud Archive quasars, and this might explain why the LBQS radio-loud quasars are in sparser environments.

The authors would like to thank H. Lin for kind assistance in utilizing CNO2 results and for comparing PPP with SExtractor. This work was partially supported by NASA through GO program 5450 from the Space Telescope Science Institute, which is operated by the Association of Universities for Research in Astronomy, Inc., under NASA contract NAS 5-26555. This research has made use of the NASA/IPAC Extragalactic Database (NED) which is operated by the Jet Propulsion Laboratory, California Institute of Technology, under contract with the National Aeronautics and Space Administration. RAF acknowledges support from the UA/NASA Spacegrant Fellowship, NSF grant AST-9623788, and NGT-5-50283, the latter a NASA Graduate Student Researchers Program Fellowship. EJH acknowledges support from NASA grants NAGW-3134 and NGT-51152, the latter a NASA Graduate Student Researchers Program Fellowship at the University of Arizona.



## REFERENCES

- Bahcall, J. N., Kirhakos, S., Saxe, D. H., & Schneider, D. P. 1997, *ApJ*, 479, 642
- Bertin, E., & Arnouts, S. 1996, *A&A*, 117, 393
- Bischof, O. B., & Becker, R. H. 1997, *AJ*, 113, 2000
- Blandford, R. D. 1990, in *Active Galactic Nuclei*, ed. T. J.-L. Courvoisier, & M. Mayor (Berlin: Springer), 161
- Boyce, P. J. et al. 1998, *MNRAS*, 298, 121
- Boyce, P. J., Disney, M. J., & Bleaden, D. G. 1999, *MNRAS*, 302, L39
- Brinkman, W., Laurent-Muehleisen, S. A., Voges, W., Seibert, J., Becker, R. H., Brotherton, M. S., White, R. L., & Gregg, M. D. 2000, *A&A*, 356, 445
- Casertano, S., Ratnatunga, R. E., Im, M., Neuschaefer, L. W., Ostrander, E. J., & Windhorst, R. A. 1995, *ApJ*, 453, 499
- Cristiani, S., & Vio, R. 1990, *A&A*, 227, 385
- Coleman, G. D., Wu, C., & Weedman, D. W. 1980, *ApJS*, 43, 393
- Davis, M., & Peebles, P. J. E. 1983, *ApJ*, 267, 465
- Disney, M. J. et al. 1995, *Nature*, 376, 150
- Dressler, A. 1980, *ApJ*, 236, 351
- Ellingson, E., Yee, H. K. C., & Green, R. F. 1991, *ApJ*, 371, 49
- Fisher, K., Bahcall, J., Kirhakos, S., & Schneider, D. 1996, *ApJ*, 468, 469
- Foltz, C. B., Chaffee, F. H., Hewett, P. C., MacAlpine, G. M., Turnshek, D. A., Weymann, R. J., & Anderson, S. F. 1987, *AJ*, 94, 1423
- French, H. B., & Gunn, J. E. 1983, *ApJ*, 269, 29
- Gehren, T., Fried, J., Wehinger, P. A., & Wyckoff, S. 1984, *ApJ*, 278, 11
- Goldschmidt, P., Kukula, M. J., Miller, L., & Dunlop, J. S. 1999, *ApJ*, 511, 612
- Goldschmidt, P. & Miller, L. 1998, *MNRAS*, 293, 107
- Griffiths, R. E. et al. 1994a, *ApJ*, 435, L19
- Griffiths, R. E. et al. 1994b, *ApJ*, 437, 67

- Hall, P. B., & Green, R. F. 1998, *ApJ*, 507, 558
- Hewett, P. C., Foltz, C. B., & Chaffee, F. H. 1995, *AJ*, 109, 1498
- Hewitt, A., & Burbidge, G. 1989, *ApJS*, 69, 1
- Hill, G. J., & Lilly, S. J. 1991, *ApJ*, 367, 1
- Hooper, E. J., Impey, C. D., Foltz, C. B., & Hewett, P. C. 1996 *ApJ*, 473, 746
- Hooper, E. J., Impey, C. D., & Foltz, C. B. 1997, *ApJ*, 480, L95
- Holtzman, J. A., Burrows, C. J., Casertano, S., Hester, J. J., Trauger, J. T., Watson, A. M., & Worthey, G. 1995, *PASP*, 107, 1065
- Köhler, T, Groote, D., Reimers, E., & Wisotzki, L. 1997, *A&A*, 325, 502
- La Franca, F., Gregorini, L., Cristiani, S., de Ruiter, H., Owen, F. 1994, *AJ*, 108, 1548
- Lanzetta, K. M. et al. 1997, *AJ*, 114, 1337
- Lin, H., Yee, H. K. C., Carlberg, R. G., Morris, S. L., Sawicki, M., Patton, D. R., Wirth, G., & Shepherd, C. W. 1999, *ApJ*, 518, 533
- Longair, M. S., & Seldner, M. 1979, *MNRAS*, 189, 433
- Malkan, M. 1984, *ApJ*, 287, 555
- McClure, R. J., Kukula, M. J., Dunlop, J. S., Baum, S. A., O’Dea, C. P., & Hughes, D. H. 1999, *MNRAS*, 308, 377
- McClure, R. J., & Dunlop, J. S. 2000, *MNRAS*, submitted, (astro-ph/0007219)
- Sanchez, S. F., & Gonzalez-Serrano, J. I. 1999, *A&A*, 352, 383
- Schade, D. J., Boyle, B. J., & Letawsky, M. 2000, *MNRAS*, 315, 498
- Seldner, M., & Peebles, P. J. E. 1978, *ApJ*, 225, 7
- Smith, E. P., & Heckman, T. M. 1990, *ApJ*, 348, 38
- Smith, E. P., Heckman, T. M., Bothun, G. D., Romanishin, W., & Balick, B. 1986, *ApJ*, 306, 64
- Smith, R. J., Boyle, B. J., & Maddox, S. J. 1995, *MNRAS*, 277, 270
- Stoche, J. T., Morris, S. L., Weymann, R. J., & Foltz, C. B. 1992, *ApJ*, 396, 487
- Stockton, A. 1982, *ApJ*, 257, 33
- Wampler, E. J., & Ponz, D. 1985, *ApJ*, 298, 448

- Weymann, R. J., Butcher, H. R., Boroson, T. A., & Peterson, B. M. 1978, *ApJ*, 226, 603
- Wilson, A. S., & Colbert, E. J. M. 1995, *ApJ*, 438, 62
- Wold, M., Lacy, M., Lilje, P. B., & Serjeant, S. 2000, *MNRAS*, 316, 267
- Wold, M., Lacy, M., Lilje, P. B., & Serjeant, S. 2001, *astro-ph/0011394*
- Yee, H. K. C. 1987, *AJ*, 94, 1461
- Yee, H. K. C. 1991, *PASP*, 103, 396
- Yee, H. K. C., & Ellingson, E. 1993, *ApJ*, 411, 43
- Yee, H. K. C., & Green, R. F. 1984, *ApJ*, 280, 79
- Yee, H. K. C., & Green, R. F. 1987, *ApJ*, 319, 28
- Yee, H. K. C., Green, R. F., & Stockman, H. S. 1986, *ApJS*, 62, 681
- Zabludoff, A. I., & Mulchaey, J. S. 1998, *ApJ*, 496, 39

Fig. 1.— Absolute magnitude,  $M_V$ , for the entire quasar sample versus redshift. The LBQS absolute magnitudes are derived from published  $B_J$  magnitudes (Hewett et al. 1995), and  $M_V$  was calculated using color and  $k$ -corrections from Cristiani & Vio (1990). For the Archive sample,  $M_V$  was calculated using  $V$  magnitudes from Hewitt & Burbidge (1989) and  $k$ -corrections from Cristiani & Vio (1990). Radio-loud quasars are represented with filled symbols, and radio-quiet quasars are represented with open symbols. The LBQS quasars are represented by triangles, and the  $F606W$  and  $F702W$  quasars are represented by squares and pentagons, respectively.

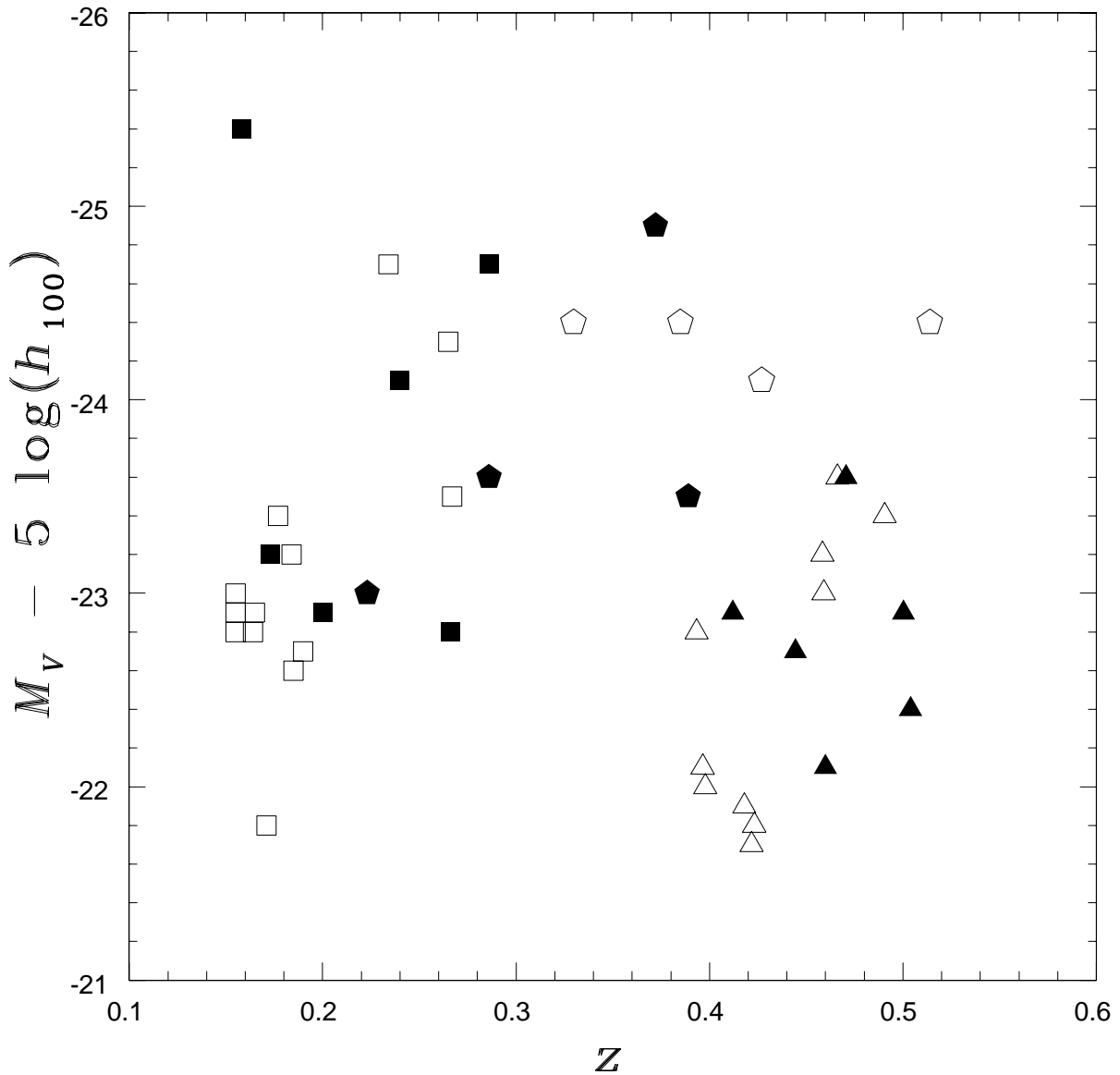


Fig. 2.— SExtractor classifier index (1=unresolved) versus magnitude for the entire LBQS  $F675W$  dataset. Triangles represent WF data; open circles represent PC data. A classifier index of 1 represents a star and 0 a galaxy; objects with indices below 0.4 are considered galaxies. PC data with indices falling between 0.5 and 0.95 correspond to the quasars.

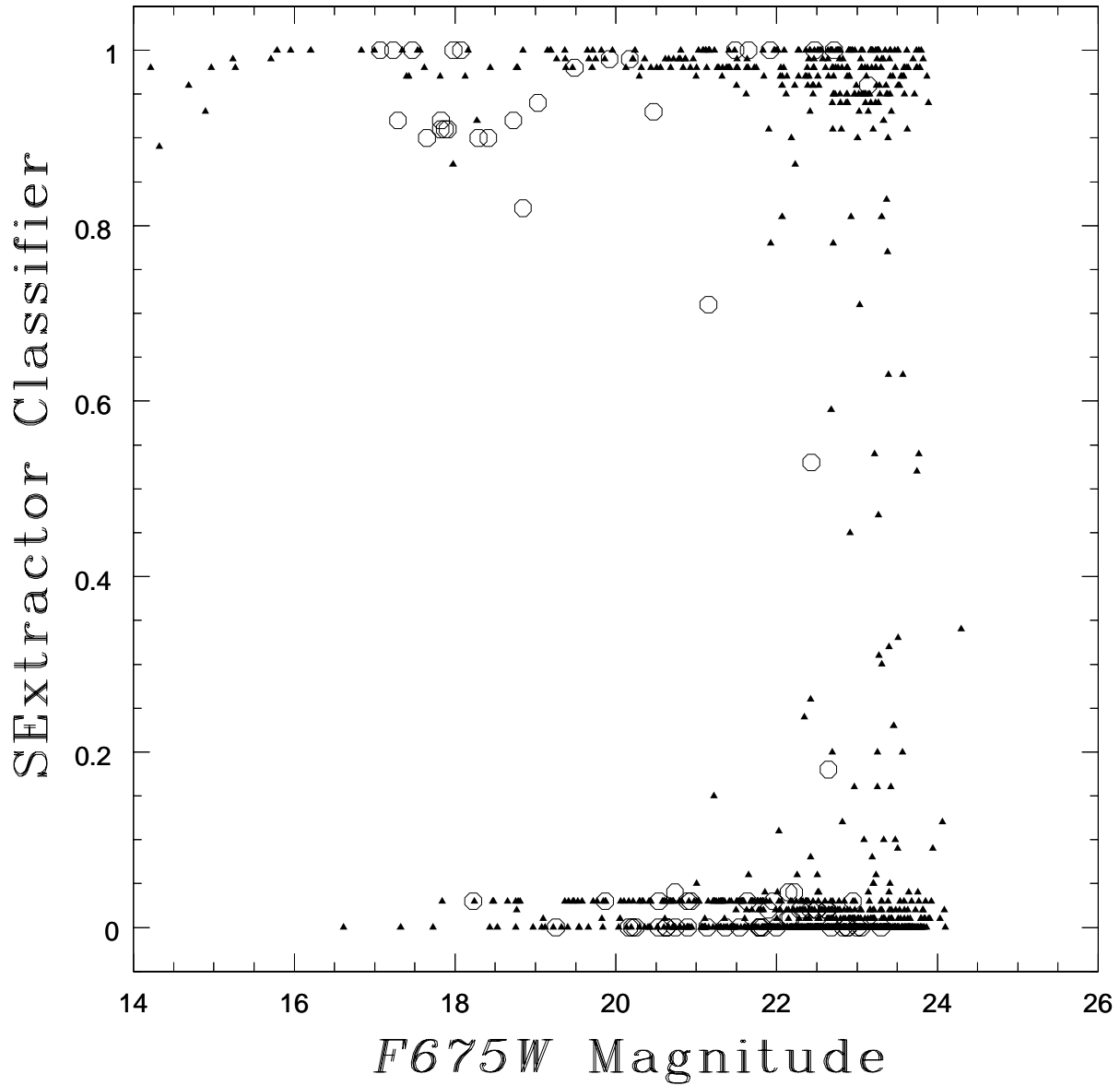


Fig. 3.— (a) Input (solid) distribution of artificial galaxies with the distribution of galaxies recovered by SExtractor (dotted) for a 1200 second  $F675W$  PC image. The data are binned  $2 \times 2$ . SExtractor detection parameters include a threshold of  $1.0\sigma$  per pixel and a minimum object area of 32 pixels. (b) Completeness versus magnitude. No galaxies with  $m_{F675W} > 22$  are used in this analysis.

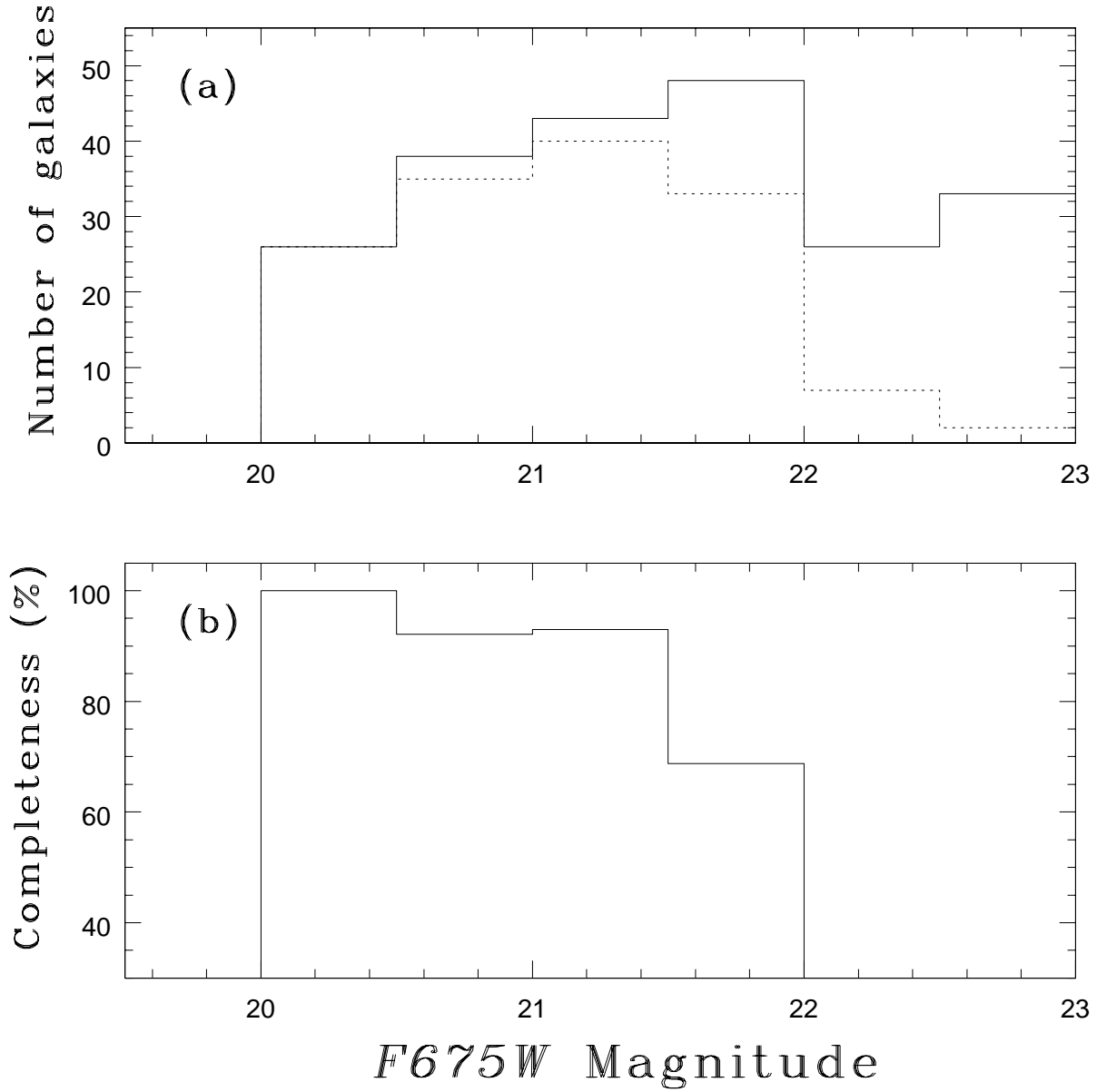


Fig. 4.— Observed galaxy counts per square degree (triangles) with the integrated luminosity function (solid line) derived from CNOC2 galaxy survey (Lin et al. 1999). Panels (a), (b) and (c) show the results for the CNOC2  $R_c$ ,  $V$  and Medium Deep Survey  $F555W$  (Casertano et al. 1995) counts, and the integrated luminosity function matches survey data well. Panels (d), (e) and (f) show the galaxy counts derived from WFPC2 images of quasar fields. The integrated luminosity function matches the  $F675W$  galaxy counts, but the quasars imaged in the  $F606W$  and  $F702W$  filters show excess counts. Error bars are  $1\sigma$  Poisson errors.

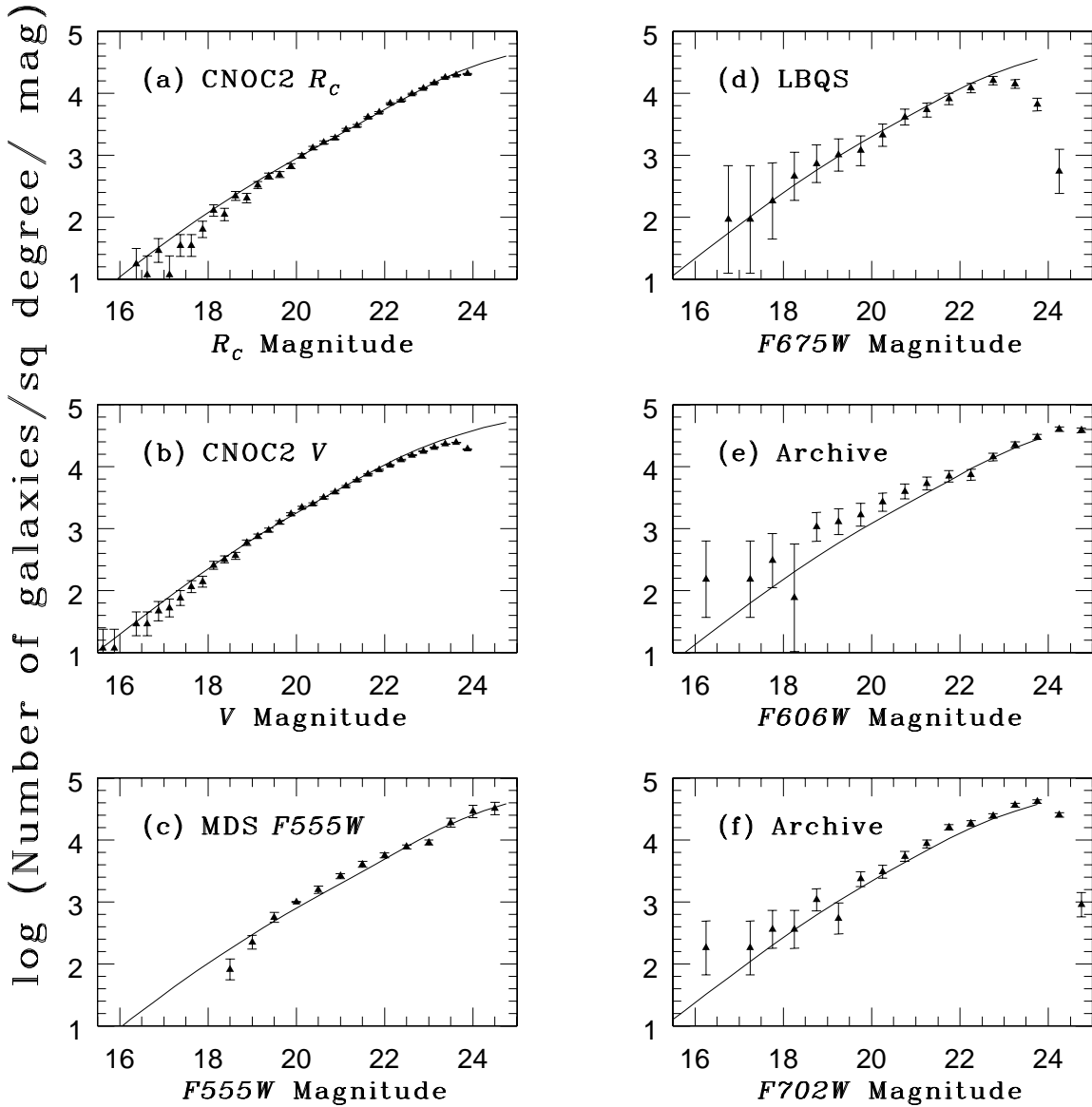


Fig. 5.— Average number of excess galaxies per field versus angular distance from the quasar for the (a) Archive and (b) LBQS samples. Error bars are  $1\sigma$  Poisson errors. The Archive sample shows an excess above background, but the LBQS dataset shows no significant excess.

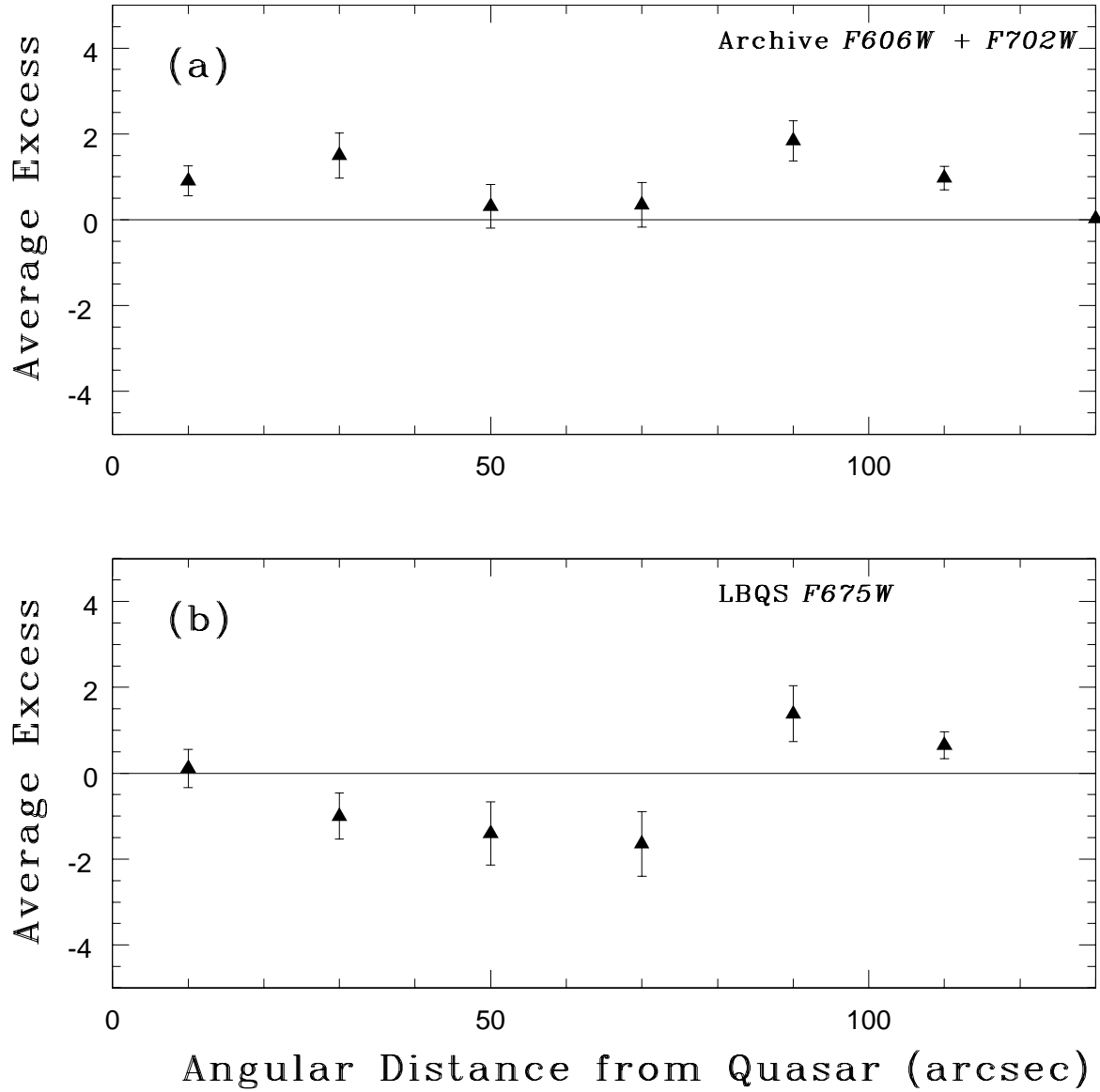




Fig. 6.— Average number of excess galaxies per field versus projected distance to quasar for the (a) Archive and (b) LBQS quasar samples. The Archive quasars show a centrally-concentrated excess above background out to  $300 h_{100}^{-1}$  kpc; the LBQS quasars show no excess. Error bars are  $1\sigma$  Poisson errors.

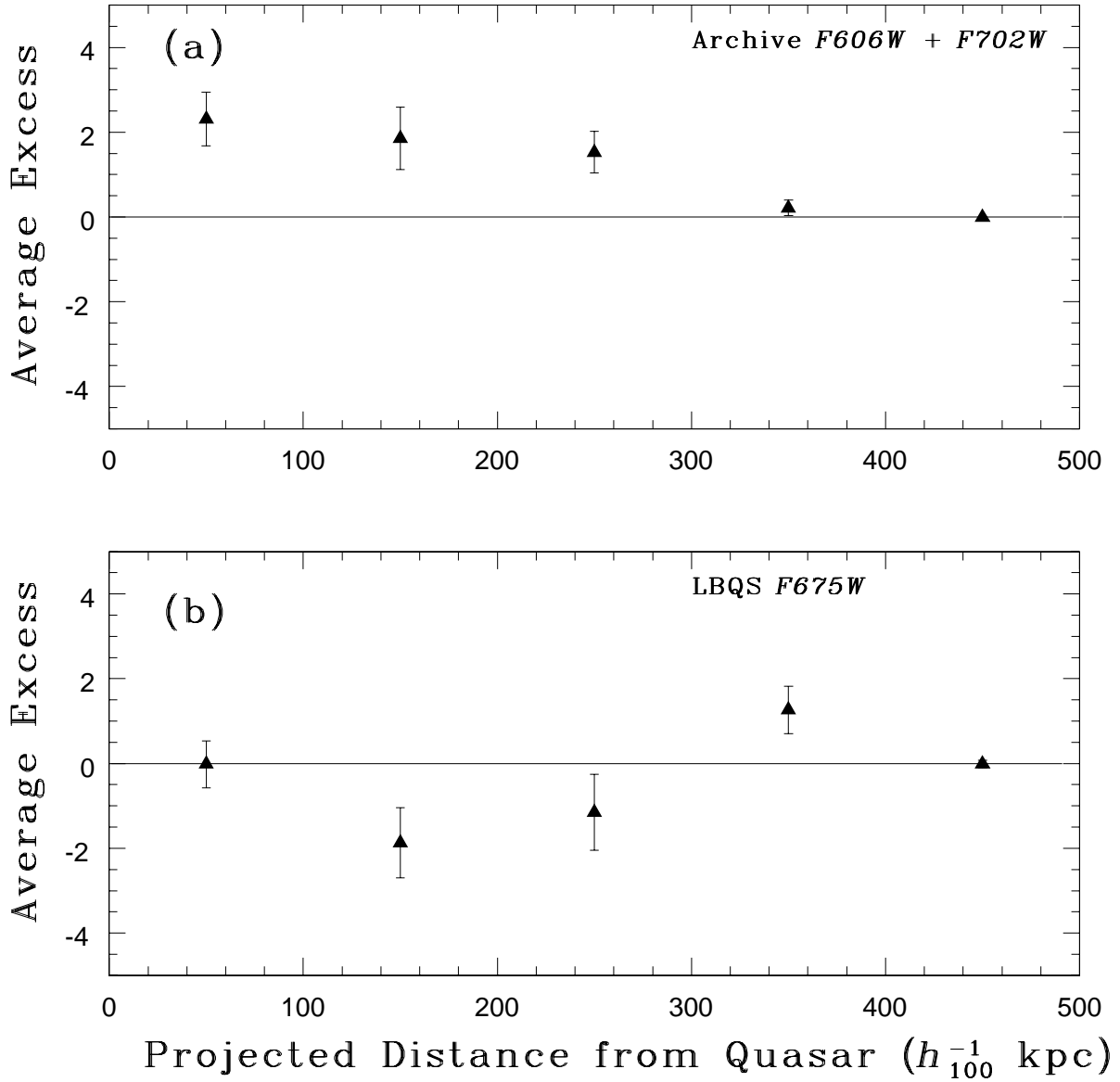


Fig. 7.—  $B_{gq}$  versus redshift for the entire sample of quasars. Radio-loud quasars are represented with filled symbols, and radio-quiet quasars are represented with open symbols. The LBQS quasars are represented by triangles, and the  $F606W$  and  $F702W$  quasars are represented by squares and pentagons, respectively. There is no evidence for a radio dichotomy, and  $B_{gq}$  values for the LBQS sample lie systematically below the values of the Archive sample.

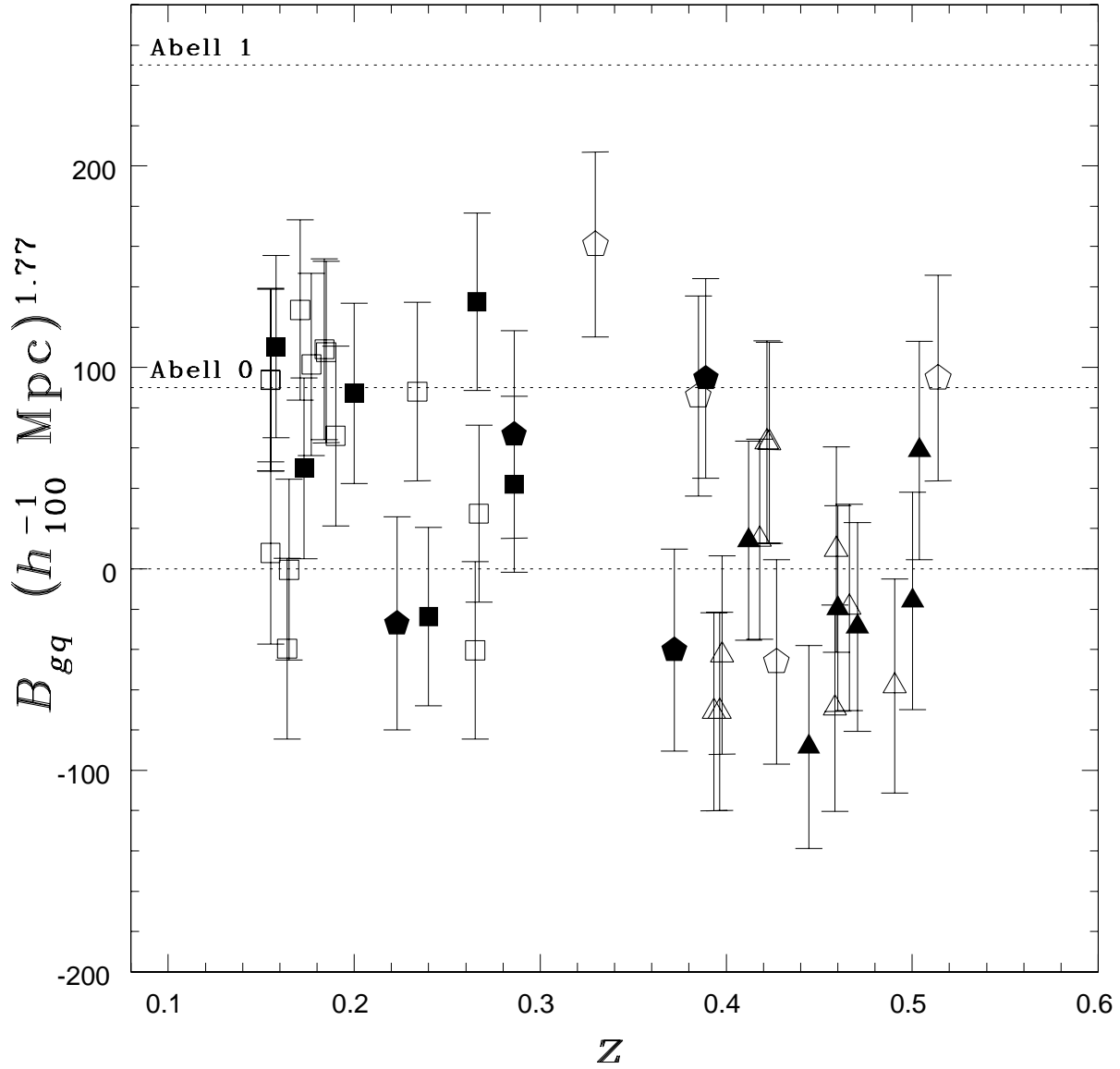


Fig. 8.—  $B_{gq}$  versus redshift, with Archive  $B_{gq}$  values recalculated using only  $m_* - 1 < m < m_* + 1.4$  galaxies to mimic the completeness of the LBQS images. Radio-loud quasars are represented with filled symbols, and radio-quiet quasars are represented with open symbols. The LBQS quasars are represented by triangles, and the  $F606W$  and  $F702W$  quasars are represented by squares and pentagons, respectively. Again, the LBQS sample lies systematically below the values of the Archive sample.

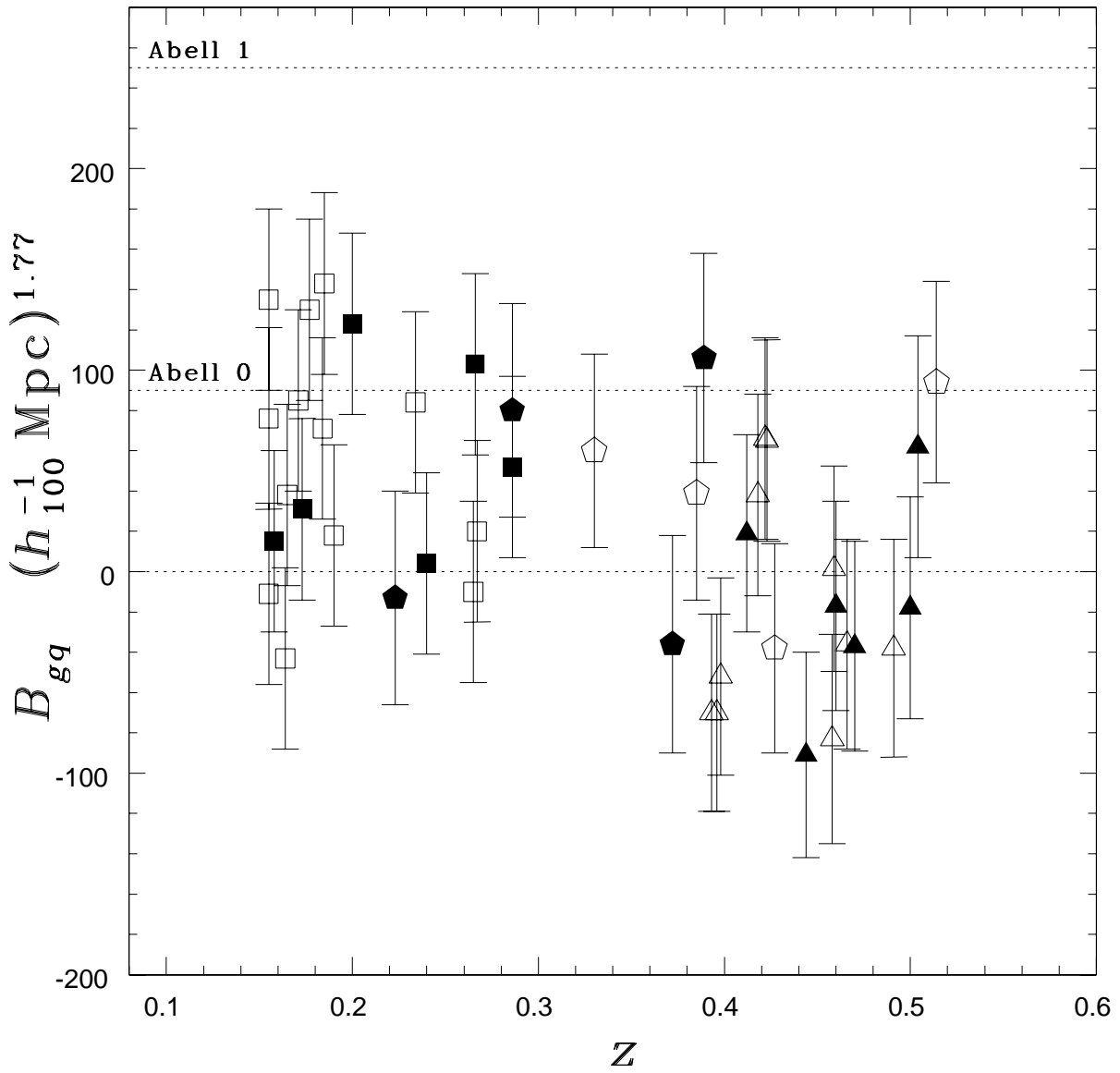




Fig. 10.— Radio power at 5GHz versus  $B_{gq}$  for quasars with available radio data. The LBQS quasars are represented by triangles and upper limits, and the  $F606W$  and  $F702W$  quasars are represented by squares and pentagons, respectively. We find no correlation between radio power and environment when considering both radio-loud and quiet quasars. However, when considering the radio-loud quasars only, a Spearman rank test indicates a 95% probability that radio power is positively correlated with environment.

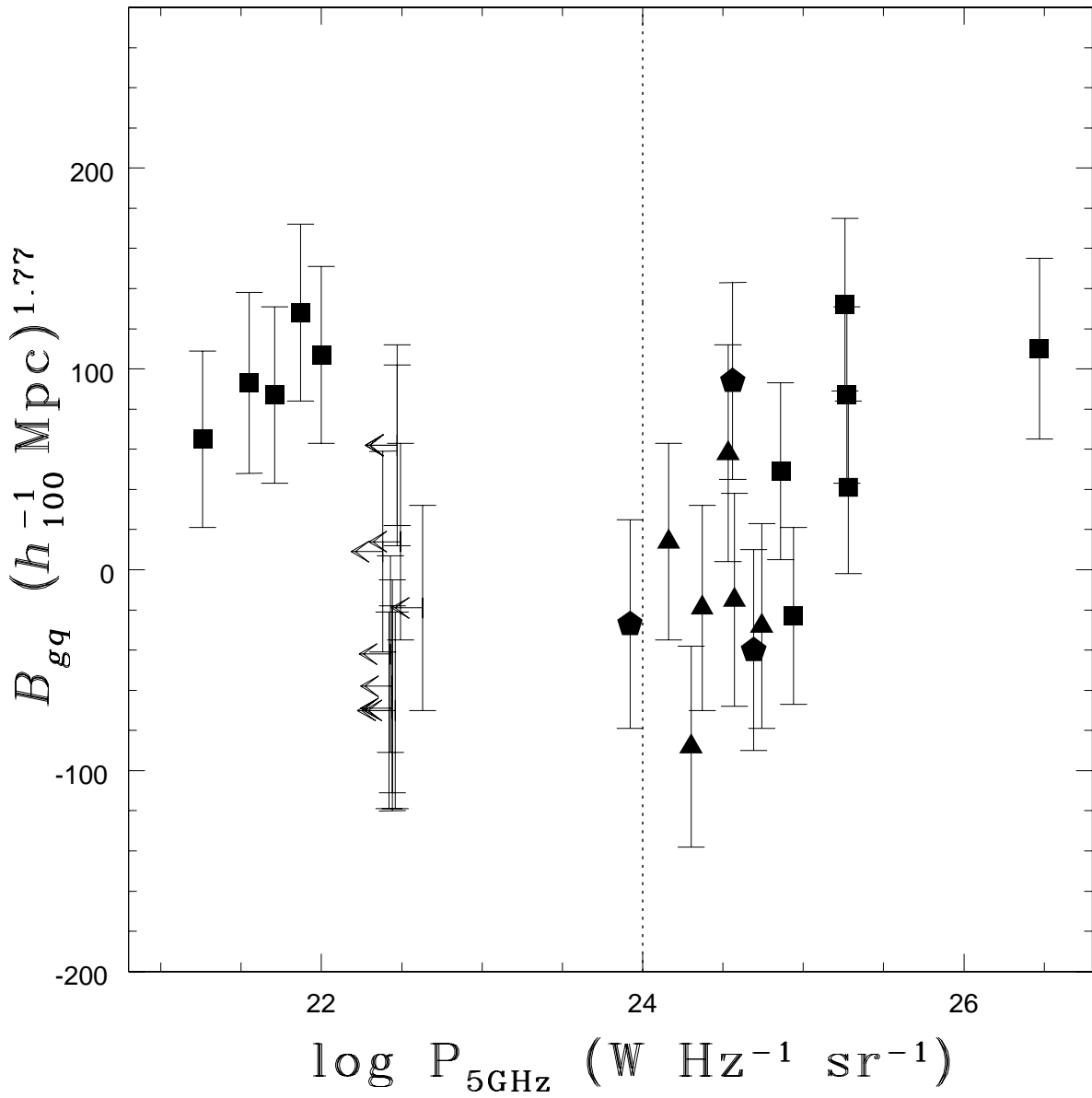


Table 1. LBQS Sample

Name	$z$	$B_J^a$	$M_V^b$	RL/RQ	$\log(P_{5\text{GHz}}^c)$	Filter	$t_{\text{total}}$ (sec)	$N_{\text{exp}}$
0020+0018	0.4232	18.60	−21.83	RQ	<22.47	F675W	1200	3
0021−0301	0.4218	18.77	−21.65	RQ	<22.47		1200	3
0100+0205	0.3934	17.51	−22.78	RQ	<22.42		1280	4
1138+0003	0.5003	17.90	−22.85	RL	24.57		1280	4
1149+0043	0.4661	17.04	−23.56	RQ	<22.63		1480	5
1209+1259	0.4180	18.55	−21.86	RQ	<22.49		1200	3
1218+1734	0.4445	17.78	−22.74	RL	24.30		1200	3
1222+1010	0.3978	18.33	−21.97	RQ	<22.43		1200	3
1222+1235	0.4121	17.43	−22.94	RL	24.16		1200	3
1230−0015	0.4705	17.00	−23.62	RL	24.64		1580	5
1240+1754	0.4584	17.41	−23.16	RQ	<22.44		1480	5
1242−0123	0.4906	17.33	−23.38	RQ	<22.44		1280	4
1243+1701	0.4591	17.61	−22.97	RQ	<22.38		1400	4
2214−1903	0.3965	18.16	−22.14	RQ	<22.46		1280	4
2348+0210	0.5039	18.35	−22.41	RL	24.53		1280	4
2351−0036	0.4600	18.47	−22.11	RL	24.37		1200	3

<sup>a</sup> $B_J$  magnitudes are from Hewett et al. (1995).

<sup>b</sup> $M_V$  is calculated from  $B_J$  using color and k-corrections from Cristiani & Vio (1990).

<sup>c</sup>Units of  $\text{W Hz}^{-1} \text{sr}^{-1}$ . Assumes  $H_0 = 50 \text{ km s}^{-1} \text{Mpc}^{-1}$ . The 8.4 GHz data from Hooper et al. (1997) are converted to 5 GHz using a spectral index of  $-0.32$ .

Table 2. HST Archive Sample

Name	$z$	$V^a$	$M_V^b$	RL/RQ	$\log(P_{5\text{GHz}}^c)$	Filter	$t_{\text{total}}$ (sec)	$N_{\text{exp}}$	Ref.
PG 0052+251	0.155	15.42	−22.8	RQ	21.55	F606W	2100	3	1
HB89 0205+024	0.155	15.39	−22.9	RQ	...		2100	3	
Q 0316−346	0.265	15.2	−24.3	RQ	...		2100	3	
PG 0923+201	0.190	16.04	−22.7	RQ	21.26		2100	3	
PG 0953+414	0.234	14.5	−24.7	RQ	21.71		1800	3	
PKS 1004+13	0.240	15.15	−24.1	RL	24.94		2100	3	
PG 1012+008	0.185	16.0	−22.6	RQ	22.00		2100	3	
PG 1116+215	0.177	15.17	−23.4	RQ	...		1800	3	
PG 1202+281	0.165	15.51	−22.9	RQ	...		1800	3	
PG 1226+023 <sup>d</sup>	0.158	12.86	−25.4	RL	26.47		1800	3	
PKS 1302−102	0.286	14.92	−24.7	RL	25.28		1800	3	
PG 1307+085	0.155	15.28	−23.0	RQ	...		2100	3	
PG 1309+355	0.184	15.45	−23.2	RQ	...		2100	3	
PG 1402+261	0.164	15.57	−22.8	RQ	...		2100	3	
PG 1444+407	0.267	15.95	−23.5	RQ	...		1800	3	
PG 1545+210 <sup>e</sup>	0.266	16.69	−22.8	RL	25.26		1800	3	
PKS 2135−14	0.200	15.91	−22.9	RL	25.27		2100	3	
PKS 2349−01	0.173	15.33	−23.2	RL	24.86		2100	3	
PHL 909	0.171	16.7	−21.8	RQ	21.87		2100	3	
PG 0043+039	0.385	15.88	−24.4	RQ	...	F702W	1800	4	2
PKS 0202−76	0.389	16.77	−23.5	RL	24.56		1800	4	2
PKS 0312−77	0.223	16.10	−23.0	RL	23.92		1800	4	2
IRAS 04505−2958	0.286	16.0	−23.6	RL	...		1800	4	3
HB 0850+440	0.514	16.4	−24.4	RQ	...		2400	3	4
PG 1001+291	0.330	15.51	−24.4	RQ	...		2400	3	5
PG 1358+043	0.427	16.31	−24.1	RQ	...		1800	4	2
PG 1704+608	0.372	15.28	−24.9	RL	24.69		1800	4	2

<sup>a</sup> $V$  magnitudes are from Hewitt & Burbidge (1989).

<sup>b</sup> $M_V$  is calculated from  $V$  using k-corrections from Cristiani & Vio (1990).

<sup>c</sup>Units of  $\text{W Hz}^{-1} \text{sr}^{-1}$ . Assumes  $H_0 = 50 \text{ km s}^{-1} \text{Mpc}^{-1}$ . The  $F606W$  data are from McLure & Dunlop (2000).

<sup>d</sup>3C273

<sup>e</sup>3C323.1

References. — (1) Fisher et al. 1996; (2) Boyce et al. 1998; (3) Disney et al. 1995; (4) Lanzetta et al. 1997; (5) Boyce, Disney, & Bleaden 1999

Table 3. Galaxy Counts and Clustering for LBQS Sample

Name	z	$\theta_{max}$ (")	$r_{max}$ ( $h_{100}^{-1}$ kpc)	$14 < m < 22$							$m_* - 1 < m < m_* + 2$				
				$N_{obs}$	$N_{exp}$	$N_{excess}$	$\delta$	$B_{gg}^a$	$m_*$	$N_{obs}$	$N_{exp}$	$N_{excess}$	$\delta$	$B_{gg}^a$	
LBQS 0020+0018	0.423	130.3	430	25	$17.8 \pm 5.5$	$7.2 \pm 5.5$	0.40	$65 \pm 49$	20.4	23	$16.4 \pm 5.3$	$6.6 \pm 5.3$	0.40	$62 \pm 49$	
LBQS 0021-0301	0.422	131.7	434	25	$17.8 \pm 5.5$	$7.2 \pm 5.5$	0.40	$65 \pm 50$	20.4	23	$16.4 \pm 5.3$	$6.6 \pm 5.3$	0.40	$62 \pm 50$	
LBQS 0100+0205	0.393	130.6	416	10	$17.8 \pm 5.5$	$-7.8 \pm 5.5$	-0.44	$-69 \pm 48$	20.3	9	$16.6 \pm 5.3$	$-7.6 \pm 5.3$	-0.46	$-70 \pm 49$	
LBQS 1138+0003 <sup>b</sup>	0.500	130.4	464	16	$17.8 \pm 5.5$	$-1.8 \pm 5.5$	-0.10	$-18 \pm 55$	20.9	14	$15.5 \pm 5.1$	$-1.5 \pm 5.1$	-0.10	$-15 \pm 53$	
LBQS 1149+0043	0.466	128.9	445	14	$17.8 \pm 5.5$	$-3.8 \pm 5.5$	-0.22	$-36 \pm 51$	20.7	14	$15.9 \pm 5.2$	$-1.9 \pm 5.2$	-0.12	$-19 \pm 51$	
LBQS 1209+1259	0.418	129.9	426	22	$17.8 \pm 5.5$	$4.2 \pm 5.5$	0.23	$37 \pm 49$	20.4	18	$16.4 \pm 5.3$	$1.6 \pm 5.3$	0.10	$14 \pm 49$	
LBQS 1218+1734 <sup>b</sup>	0.444	129.8	438	8	$17.8 \pm 5.5$	$-9.8 \pm 5.5$	-0.55	$-90 \pm 50$	20.6	7	$16.2 \pm 5.2$	$-9.2 \pm 5.2$	-0.57	$-88 \pm 50$	
LBQS 1222+1010	0.398	130.3	418	12	$17.8 \pm 5.5$	$-5.8 \pm 5.5$	-0.33	$-52 \pm 49$	20.3	12	$16.6 \pm 5.3$	$-4.6 \pm 5.3$	-0.28	$-42 \pm 49$	
LBQS 1222+1235 <sup>b</sup>	0.412	130.1	424	20	$17.8 \pm 5.5$	$2.2 \pm 5.5$	0.12	$19 \pm 49$	20.4	18	$16.5 \pm 5.3$	$1.5 \pm 5.3$	0.09	$14 \pm 49$	
LBQS 1230-0015 <sup>b</sup>	0.470	130.1	451	14	$17.8 \pm 5.5$	$-3.8 \pm 5.5$	-0.22	$-36 \pm 52$	20.7	13	$15.9 \pm 5.2$	$-2.9 \pm 5.2$	-0.18	$-28 \pm 51$	
LBQS 1240+1754	0.458	130.3	447	9	$17.8 \pm 5.5$	$-8.8 \pm 5.5$	-0.50	$-83 \pm 51$	20.6	9	$16.0 \pm 5.2$	$-7.0 \pm 5.2$	-0.44	$-69 \pm 51$	
LBQS 1242-0123	0.491	130.2	459	14	$17.8 \pm 5.5$	$-3.8 \pm 5.5$	-0.22	$-37 \pm 54$	20.8	10	$15.6 \pm 5.1$	$-5.6 \pm 5.1$	-0.36	$-58 \pm 53$	
LBQS 1243+1701	0.459	129.1	443	18	$17.8 \pm 5.5$	$0.2 \pm 5.5$	0.01	$1 \pm 51$	20.6	17	$16.0 \pm 5.2$	$1.0 \pm 5.2$	0.06	$9 \pm 50$	
LBQS 2214-1903	0.396	130.4	417	10	$17.8 \pm 5.5$	$-7.8 \pm 5.5$	-0.44	$-70 \pm 49$	20.3	9	$16.6 \pm 5.3$	$-7.6 \pm 5.3$	-0.46	$-70 \pm 49$	
LBQS 2348+0210 <sup>b</sup>	0.504	130.6	466	24	$17.8 \pm 5.5$	$6.2 \pm 5.5$	0.35	$62 \pm 55$	20.9	21	$15.5 \pm 5.1$	$5.5 \pm 5.1$	0.36	$58 \pm 54$	
LBQS 2351-0036 <sup>b</sup>	0.460	129.4	444	16	$17.8 \pm 5.5$	$-1.8 \pm 5.5$	-0.10	$-17 \pm 51$	20.7	14	$16.0 \pm 5.2$	$-2.0 \pm 5.2$	-0.13	$-19 \pm 51$	
Average					$16.1 \pm 5.6$	$-1.8 \pm 1.4^c$	-0.10	$-16 \pm 12^c$		$14.4 \pm 5.0$		$-1.7 \pm 1.3^c$	-0.10	$-16 \pm 12^c$	
Radio Loud								$-13 \pm 21^c$						$-13 \pm 21^c$	
Radio Quiet								$-17 \pm 16^c$						$-18 \pm 15^c$	

<sup>a</sup>Units of ( $h_{100}^{-1}$  Mpc)<sup>1.77</sup>. Error calculations are described in text.

<sup>b</sup>Radio-Loud Quasars

<sup>c</sup>Error is  $\sqrt{\frac{\sum \sigma_i^2}{n}}$



Table 4. Galaxy Counts and Clustering for *F606W* Archive Sample

Name	$z$	$\theta_{max}$ ( $''$ )	$r_{max}$ ( $h_{100}^{-1}$ kpc)	$N_{obs}$	$14 < m < 22$					$m_* - 1 < m < m_* + 2$				
					$N_{exp}$	$N_{excess}$	$\delta$	$B_{gg}^a$	$m_*$	$N_{obs}$	$N_{exp}$	$N_{excess}$	$\delta$	$B_{gg}^a$
PG 0052+251	0.155	119.0	208	19	$10.9 \pm 4.3$	$8.1 \pm 4.3$	0.74	$93 \pm 49$	18.5	7	$2.6 \pm 2.1$	$4.4 \pm 2.1$	1.66	$93 \pm 45$
HB89 0205+024	0.155	119.6	209	10	$10.9 \pm 4.3$	$-0.9 \pm 4.3$	-0.08	$-10 \pm 49$	18.5	3	$2.6 \pm 2.1$	$0.4 \pm 2.1$	0.14	$7 \pm 45$
Q 0316-346	0.265	119.6	304	6	$10.9 \pm 4.3$	$-4.9 \pm 4.3$	-0.45	$-49 \pm 43$	19.8	5	$8.5 \pm 3.8$	$-3.5 \pm 3.8$	-0.41	$-40 \pm 44$
PG 0923+201	0.190	118.1	240	20	$10.9 \pm 4.3$	$9.1 \pm 4.3$	0.83	$96 \pm 45$	19.0	8	$4.1 \pm 2.6$	$3.9 \pm 2.6$	0.95	$65 \pm 44$
PG 0953+414	0.234	121.3	285	23	$10.9 \pm 4.3$	$12.1 \pm 4.3$	1.11	$122 \pm 43$	19.5	13	$6.5 \pm 3.3$	$6.5 \pm 3.3$	1.02	$87 \pm 44$
PKS 1004+13 <sup>b</sup>	0.240	119.6	286	5	$10.9 \pm 4.3$	$-5.9 \pm 4.3$	-0.54	$-60 \pm 43$	19.5	5	$6.8 \pm 3.4$	$-1.8 \pm 3.4$	-0.27	$-23 \pm 44$
PG 1012+008	0.185	119.4	238	21	$10.9 \pm 4.3$	$10.1 \pm 4.3$	0.92	$108 \pm 46$	18.9	10	$3.9 \pm 2.6$	$6.1 \pm 2.6$	1.58	$107 \pm 44$
PG 1116+215	0.177	121.9	235	20	$10.9 \pm 4.3$	$9.1 \pm 4.3$	0.83	$99 \pm 47$	18.8	9	$3.5 \pm 2.4$	$5.5 \pm 2.4$	1.56	$101 \pm 45$
PG 1202+281	0.165	121.8	223	17	$10.9 \pm 4.3$	$6.1 \pm 4.3$	0.56	$67 \pm 47$	18.7	3	$3.0 \pm 2.3$	$-0.0 \pm 2.3$	-0.01	$0 \pm 44$
PG 1226+023 <sup>b</sup>	0.158	119.8	212	20	$10.9 \pm 4.3$	$9.1 \pm 4.3$	0.83	$103 \pm 49$	18.6	8	$2.7 \pm 2.2$	$5.3 \pm 2.2$	1.91	$110 \pm 45$
PKS 1302-102 <sup>b</sup>	0.286	119.4	319	15	$10.9 \pm 4.3$	$4.1 \pm 4.3$	0.37	$41 \pm 43$	20.0	14	$10.0 \pm 4.1$	$4.0 \pm 4.1$	0.39	$41 \pm 43$
PG 1307+085	0.155	123.1	215	24	$10.9 \pm 4.3$	$13.1 \pm 4.3$	1.20	$150 \pm 49$	18.5	7	$2.6 \pm 2.1$	$4.4 \pm 2.1$	1.66	$93 \pm 45$
PG 1309+355	0.184	119.2	237	17	$10.9 \pm 4.3$	$6.1 \pm 4.3$	0.56	$65 \pm 46$	18.9	10	$3.8 \pm 2.5$	$6.2 \pm 2.5$	1.61	$108 \pm 44$
PG 1402+261	0.164	118.7	216	8	$10.9 \pm 4.3$	$-2.9 \pm 4.3$	-0.27	$-32 \pm 48$	18.7	1	$3.0 \pm 2.2$	$-2.0 \pm 2.2$	-0.66	$-39 \pm 44$
PG 1444+407	0.267	119.3	305	11	$10.9 \pm 4.3$	$0.1 \pm 4.3$	0.01	$0 \pm 43$	19.8	11	$8.6 \pm 3.8$	$2.4 \pm 3.8$	0.28	$27 \pm 43$
PG 1545+210 <sup>b</sup>	0.266	118.3	302	22	$10.9 \pm 4.3$	$11.1 \pm 4.3$	1.01	$111 \pm 43$	19.8	20	$8.5 \pm 3.8$	$11.5 \pm 3.8$	1.34	$132 \pm 43$
PKS 2135-14 <sup>b</sup>	0.200	119.9	253	16	$10.9 \pm 4.3$	$5.1 \pm 4.3$	0.47	$53 \pm 45$	19.1	10	$4.6 \pm 2.8$	$5.4 \pm 2.8$	1.18	$87 \pm 44$
PKS 2349-01 <sup>b</sup>	0.173	117.8	224	16	$10.9 \pm 4.3$	$5.1 \pm 4.3$	0.47	$55 \pm 47$	18.8	6	$3.3 \pm 2.4$	$2.7 \pm 2.4$	0.79	$49 \pm 44$
PHL 909	0.171	118.8	223	21	$10.9 \pm 4.3$	$10.1 \pm 4.3$	0.92	$110 \pm 47$	18.8	10	$3.3 \pm 2.3$	$6.7 \pm 2.3$	2.06	$128 \pm 44$
Average				$16.4 \pm 5.6$		$5.4 \pm 1.0^c$	0.50	$59 \pm 10^c$		$8.4 \pm 4.3$		$3.6 \pm 0.7^c$	0.88	$60 \pm 10^c$
Radio Loud								$50 \pm 18^c$						$66 \pm 18^c$
Radio Quiet								$63 \pm 12^c$						$57 \pm 12^c$

<sup>a</sup>Units of  $(h_{100}^{-1} \text{ Mpc})^{1.77}$ . Error calculations are described in text.

<sup>b</sup>Radio-Loud Quasars

<sup>c</sup>Error is  $\sqrt{\frac{\sum \sigma_i^2}{n}}$

Table 5. Galaxy Counts and Clustering for *F702W* Archive Sample

Name	z	$\theta_{max}$ (")	$r_{max}$ ( $h_{100}^{-1}$ kpc)	$14 < m < 22$						$m_* - 1 < m < m_* + 2$				
				$N_{obs}$	$N_{exp}$	$N_{excess}$	$\delta$	$B_{gg}^a$	$m_*$	$N_{obs}$	$N_{exp}$	$N_{excess}$	$\delta$	$B_{gg}^a$
PG 0043+039	0.385	130.2	410	29	$19.5 \pm 5.7$	$9.5 \pm 5.7$	0.49	$81 \pm 49$	20.1	28	$18.4 \pm 5.6$	$9.6 \pm 5.6$	0.52	$85 \pm 49$
PKS 0202-76 <sup>b</sup>	0.389	129.2	409	30	$19.5 \pm 5.7$	$10.5 \pm 5.7$	0.54	$89 \pm 49$	20.2	29	$18.4 \pm 5.6$	$10.6 \pm 5.6$	0.58	$94 \pm 49$
PKS 0312-77 <sup>b</sup>	0.223	130.2	296	10	$19.5 \pm 5.7$	$-9.5 \pm 5.7$	-0.49	$-88 \pm 53$	18.9	5	$6.7 \pm 3.4$	$-1.7 \pm 3.4$	-0.26	$-27 \pm 52$
IRAS 04505-2958 <sup>b</sup>	0.286	129.6	346	34	$19.5 \pm 5.7$	$14.5 \pm 5.7$	0.74	$126 \pm 50$	19.5	17	$11.3 \pm 4.4$	$5.7 \pm 4.4$	0.50	$66 \pm 51$
HB 0850+440	0.514	121.1	435	36	$19.5 \pm 5.7$	$16.5 \pm 5.7$	0.85	$149 \pm 51$	20.9	27	$17.0 \pm 5.4$	$10.0 \pm 5.4$	0.58	$94 \pm 50$
PG 1001+291	0.330	131.8	382	45	$19.5 \pm 5.7$	$25.5 \pm 5.7$	1.31	$198 \pm 44$	19.8	33	$15.2 \pm 5.1$	$17.8 \pm 5.1$	1.17	$160 \pm 45$
PG 1358+043	0.427	130.7	434	13	$19.5 \pm 5.7$	$-6.5 \pm 5.7$	-0.33	$-57 \pm 50$	20.4	13	$18.0 \pm 5.5$	$-5.0 \pm 5.5$	-0.28	$-46 \pm 50$
PG 1704+608 <sup>b</sup>	0.372	131.9	409	15	$19.5 \pm 5.7$	$-4.5 \pm 5.7$	-0.23	$-39 \pm 49$	20.1	14	$18.5 \pm 5.6$	$-4.5 \pm 5.6$	-0.24	$-40 \pm 50$
Average				$26.5 \pm 11.7$		$7.0 \pm 2.0^c$	0.36	$57 \pm 17^c$		$20.8 \pm 9.2$		$5.3 \pm 1.8^c$	0.32	$48 \pm 17^c$
Radio Loud								$22 \pm 25^c$						$23 \pm 25^c$
Radio Quiet								$92 \pm 24^c$						$73 \pm 24^c$

<sup>a</sup>Units of  $(h_{100}^{-1} \text{ Mpc})^{1.77}$ . Error calculations are described in text.

<sup>b</sup>Radio-Loud Quasars

<sup>c</sup>Error is  $\frac{\sqrt{\sum \sigma_i^2}}{n}$

Table 6. Comparison of Individual  $B_{gq}$  Values<sup>a</sup>

Object	Yee & Ellingson 1993	McLure & Dunlop 2000	This work
1004+431	$-22 \pm 24$	$-16 \pm 71$	$-23 \pm 44$
1302–102	$62 \pm 52$	$94 \pm 107$	$41 \pm 43$
1545+210	$129 \pm 66$	$113 \pm 109$	$132 \pm 43$
1704+608	$-58 \pm 41$	...	$-40 \pm 50$
2349–01	$64 \pm 44$	$179 \pm 130$	$49 \pm 44$

<sup>a</sup> $B_{gq}$  in units of  $(h_{100}^{-1} \text{ Mpc})^{1.77}$

Table 7. Comparison of Average Radio-Loud and Quiet  $B_{gq}$  Values<sup>a</sup>

Reference	Radio-Loud	N <sup>b</sup>	Radio-Quiet	N <sup>b</sup>	z
Archive F606W <sup>c</sup>	$66 \pm 18$	6	$57 \pm 12$	13	$0.155 \leq z \leq 0.286$
Archive F702W <sup>c</sup>	$23 \pm 25$	4	$73 \pm 24$	4	$0.223 \leq z \leq 0.514$
LBQS	$-13 \pm 21$	6	$-18 \pm 15$	10	$0.39 < z < 0.504$
McLure & Dunlop 2000 <sup>c</sup>	$79 \pm 15$	10	$96 \pm 22$	13	$0.086 \leq z \leq 0.286$
Wold et al. 2000	$78 \pm 22$	21	...	...	$0.5 \leq z \leq 0.8$
Fisher et al. 1996 <sup>c</sup>	$84 \pm_{27}^{33}$	6	$72 \pm_{19}^{20}$	14	$0.086 \leq z \leq 0.286$
Smith et al. 1995 <sup>d</sup>	...	...	$20 \pm_{8}^{14}$	169	$z < 0.3$
Ellingson et al. 1991	$56 \pm 22$	53	$21 \pm 12$	43	$0.3 < z < 0.6$

<sup>a</sup> $B_{gq}$  in units of  $(h_{100}^{-1} \text{ Mpc})^{1.77}$

<sup>b</sup>Number of quasars in sample

<sup>c</sup>Archive F606W and Fisher et al. samples use the same *HST* data and are identical except for one radio-quiet quasar, HE 1029–1401, which is included in the Fisher et al. sample but not in the Archive F606W sample. The McLure & Dunlop sample includes all the Archive F606W quasars and one of the Archive F702W quasars, and their analysis is based on the same *HST* data.

<sup>d</sup>Converted published value of  $\langle B_{gq} \rangle / \langle B_{gg} \rangle$  to  $\langle B_{gq} \rangle$  assuming  $\langle B_{gg} \rangle = 20 (h_{100}^{-1} \text{ Mpc})^{1.77}$